Review of criteria for the selection of probability distributions for wind speed data and introduction of the moment and L-moment ratio diagram methods, with a case study

T.B.M.J. Ouarda[1, 2*], C. Charron[2] and F. Chebana[1]

[1]INRS-ETE, National Institute of Scientific Research, 490 de la Couronne, Quebec City (QC), Canada, G1K9A9

[2]Institute Center for Water and Environment (iWater), Masdar Institute of Science and Technology, P.O. Box 54224, Abu Dhabi, UAE

*Corresponding author:

Email: touarda@masdar.ac.ae

Tel: +971 2 810 9107

April 2016

Abstract

This paper reviews the different criteria used in the field of wind energy to compare the goodness-of-fit of candidate probability density functions (pdfs) to wind speed records, and discusses their advantages and disadvantages. The moment ratio and L-moment ratio diagram methods are also proposed as alternative methods for the choice of the pdfs. These two methods have the advantage of allowing an easy comparison of the fit of several pdfs for several time series (stations) on a single diagram. Plotting the position of a given wind speed data set in these diagrams is instantaneous and provides more information than a goodness-of-fit criterion since it provides knowledge about such characteristics as the skewness and kurtosis of the station data set. In this paper, it is proposed to study the applicability of these two methods for the selection of pdfs for wind speed data. Both types of diagrams are used to assess the fit of the pdfs for wind speed series in the United Arab Emirates. The analysis of the moment ratio diagrams reveals that the Kappa, Log-Pearson type III and Generalized Gamma are the distributions that fit best all wind speed series. The Weibull represents the best distribution among those with only one shape parameter. Results obtained with the diagrams are compared with those obtained with goodness-of-fit statistics and a good agreement is observed especially in the case of the L-moment ratio diagram. It is concluded that these diagrams can represent a simple and efficient approach to be used as complementary method to goodness-of-fit criteria.

Keywords: wind speed; probability density distribution; moment ratio diagram; L-moments; goodness-of-fit criteria; adequacy statistics.

1 Introduction

The assessment of wind energy potential at a given site is often based on the use of probability density functions (pdfs) to characterize short term wind speed observations [1-16]. The selection of the appropriate pdf to model wind speed data is crucial in wind power energy applications as it reduces wind power output estimation uncertainties. Traditionally, the two-parameter Weibull (W2) is the most used pdf in studies related to wind speed data analysis [17]. While being extensively used in studies dedicated to the assessment of wind energy [18-25] , the Weibull is not able to represent every wind speed regime [26-28]. Recently, a number of studies have used a variety of other pdfs with variable levels of success [17, 22, 27-40]. The pdfs used include the Gamma (G), Inverse Gamma (IG), Inverse Gaussian (IGA), two and three-parameter Lognormal (LN2, LN3), Logistic (L), Log-logistic (LL), Gumbel (EV1), Generalized Extreme Value (GEV), three-parameter Beta (B), Pearson type III (P3), Log-Pearson type III (LP3), Burr (BR), Erlang (ER), Kappa (KAP) and Wakeby (WA) distributions. Ouarda et al. [27] found the GG and KAP to be superior to W2 in the United Arab Emirates (UAE). Mert and Karakus [34] found the Burr distribution to be more suitable than the GG or W2 for wind speed data in Antakya, Turkey.

A number of authors have proposed mixture distributions [13, 27, 28, 31, 41-46]. The mixture models were found to provide better fit in the case of distributions presenting bimodal characteristics. A model composed of two Weibull distributions is most often used [27, 31, 46-48]. Other mixture models used are the Normal-Normal, Truncated Normal-Weibull and Gamma-Weibull. Shin et al. [28] applied a large number of different mixture models to wind speed data in the UAE and concluded that the Weibull-Extreme value type-1 is the most appropriate distribution. The use of distributions generated by the maximum entropy principle is also common [13, 49-52]. These distributions have the advantage of being able to model wind regime with high percentages of null wind speeds and with bimodal distributions [50]. Non-parametric models were also proposed by a number of authors to model wind speed distribution. Qin [53] proposed to apply the kernel density concept to wind speed. This method was since adopted in a number of studies [27, 35, 54, 55].

Different goodness-of-fit criteria are traditionally used for the assessment of the adequacy of pdfs. An exhaustive review of the most used criteria is presented in this paper along with a discussion of their advantages and disadvantages. Such criteria include the log-likelihood (ln L) [27, 33, 56, 57], the Akaike and the Bayesian Information Criteria (AIC, BIC) [27, 28, 30, 42, 56], the coefficient of determination (R^2) [1, 3, 11, 12, 15-17, 21, 27, 28, 30-32, 35, 37, 39, 46, 49, 50, 58-62], the root mean square error (RMSE) [1, 2, 9, 13, 15, 16, 33, 36, 37, 39, 53, 56, 60-71], the Chi-square test statistic (χ^2) [1, 2, 13, 15, 27, 28, 32-36, 39, 40, 49, 53, 55, 57, 60, 68, 72], the Kolmogorov-Smirnov test statistic (KS) [9, 13, 27, 30, 32-35, 38-40, 53, 55, 56, 61, 69, 73-75] and the Anderson-Darling test statistic (AD) [32, 40, 50, 76].

An alternative method for the evaluation of the goodness-of-fit of pdfs, the moment ratio diagram, has been used extensively in hydro-meteorology [77]. Bobée et al. [78] pointed out that moment ratio diagrams have been used as a means to select a distribution to be used as a probability model for the fitting of a given data sample, to compare the shapes of distributions from a given set and to classify a set of distributions by separating them into a finite number of categories. With this approach, all possible values of the square of the coefficient of skewness and coefficient of kurtosis are represented in a coordinate system for each distribution. The selection of the appropriate distribution to fit a data sample is made based on the location of the data sample in the coordinate system. The main advantage of this approach is that it allows an easy comparison of the fit of several pdfs on a single diagram. Moment ratio diagrams are also easy to implement with the information and equations readily available in the literature, giving the approximate relationship between moments for popular pdfs [79, 80]. The position of a time series (i.e., a station) on the diagram is simply computed with the equations of moments.

The L-moment ratio diagram, a variant of the conventional moment ratio diagram, introduced by Hosking [81], has been used to select suitable pdfs for modeling hydro-meteorological variables in a large number of studies [79, 81-98]. Hosking and Wallis [79] presented the theoretical advantages of L-moments over conventional moments: They are able to characterize a wider range of distributions and they are more robust to the presence of outliers in the data when estimated from a sample. They also indicated that experience shows that L-moments are less subject to bias in estimation. Vogel and Fennessey [99] concluded that L-moment ratio diagrams should be preferred over moment ratio diagrams for applications in hydrology. The main reason is that L-moment estimators are nearly unbiased for all sample sizes and all distributions.

Despite its advantages, the moment ratio diagram approach has never been used for the assessment of wind speed distributions. It is proposed, in the present study, to develop the moment and L-moment ratio diagram approaches for wind speed data analysis and apply these approaches to wind speed data from the UAE. Ouarda et al. [27] evaluated the suitability of a wide selection of pdfs to fit wind speed data recorded at 7 stations at 10 m height in the UAE. The adequacy of the pdfs was evaluated using goodness-of-fit criteria. For comparison purposes, the same pdfs used in Ouarda et al. [27] for wind speed analysis are represented on the moment ratio diagrams. These pdfs include the W2, W3, EV1, G, GG, GEV, LN2, LN3, P3, LP3 and KAP. Both moment and L-moment ratio approaches are used and compared to the results obtained from goodness-of-fit criteria.

The present paper is organized as follows: Section 2 reviews the different criteria of goodness-of-fit, found in the literature, for the assessment of probability distribution functions for wind speed data. Section 3 presents the theoretical background on the conventional moment ratio diagrams and the L-moment ratio diagrams. Section 4 presents the methodology used to represent the selected pdfs on moment ratio diagrams. A case study dealing with the application of moment ratio diagrams is presented in Section 5 and the results are presented in Section 6. Finally, conclusions are given in section 7.

2 Review of the criteria used for the assessment of goodness-of-fit

A standard approach for the assessment of the goodness-of-fit is to visually compare the fit of the candidate pdfs. For that, wind speed samples are usually divided into class intervals and frequencies are represented with histograms. Candidate distributions are then superimposed on the histograms. Alternatively, plots of the cumulative probability, *P-P* plots or *Q-Q* plots are also represented. However, goodness-of-fit criteria provide an objective comparison of the candidate distributions and are extensively used along with the visual approach. This section reviews the criteria commonly used in the literature related to wind energy applications.

In general, the most used criteria are the ln L, AIC, BIC, R^2, χ^2, KS, and AD. The KS, χ^2 and AD statistics are associated to statistical tests that allow to identify if a sample is generated from a given theoretical distribution. In the context of wind speed distribution assessment, the statistics of these tests are used to compare the fit obtained by several theoretical distributions. Alternatively, assessment of the fit is also based on the ability of the model to predict wind power accurately.

2.1. Log-likelihood (ln *L*), and Akaike and Bayesian Information Criteria (AIC, BIC)

A given pdf $f_{\hat{\theta}}(x)$ fitted on a wind speed data set has distribution parameter estimates $\hat{\theta}$. ln L is then defined by:

$$\ln L = \ln\left(\prod_{i=1}^{n} f_{\hat{\theta}}(v_i)\right) \tag{1}$$

where v_i is the ith observed wind speed and n is the number of observations in the data set. A higher value of this criterion indicates a better fit of the model to the data.

AIC [100] and BIC[101] are related to the log-likelihood and are defined by:

$$\mathrm{AIC} = -2\ln\left(\prod_{i=1}^{n} f_{\hat{\theta}}(v_i)\right) + 2k \tag{2}$$

$$\mathrm{BIC} = -2\ln\left(\prod_{i=1}^{n} f_{\hat{\theta}}(v_i)\right) + k\ \ln(n) \tag{3}$$

where k is the number of parameters of the distribution to estimate. A lower value of these criteria indicates a better fit of the model to the data. These criteria take into consideration the parsimony of the model as they include a penalty term that increases with the number of parameters. For $n \geq 8$, BIC provides a stronger penalty than AIC for additional parameters.

2.2. Coefficients of determination (R^2)

R^2 is a measure of how much the variance of the observed data is explained by the model. The general form of R^2 is given by:

$$R^2 = 1 - \frac{\sum_{i=1}^{n}(y_i - x_i)^2}{\sum_{i=1}^{n}(y_i - \bar{y})^2} \tag{4}$$

where y_i is the ith observed data, x_i is the ith predicted data and n is the sample size. Alternatively, the square of the coefficient of correlation is also frequently used. 4 different versions of this statistic are presented here.

2.2.1. R^2_{PP}

R^2_{PP} is the coefficient of determination associated with the *P-P* plot defined by the model cumulative probabilities versus the empirical cumulative probabilities. An example of a *P-P* plot is given in Fig. 1a. R^2_{PP} is computed as follows:

$$R^2_{PP} = 1 - \frac{\sum_{i=1}^{n}(F_i - \hat{F}_i)^2}{\sum_{i=1}^{n}(F_i - \bar{F})^2} \tag{5}$$

where $\hat{F}_i$ is the predicted cumulative probability of the ith observed wind speed, F_i is the empirical probability of the ith observed wind speed and $\bar{F} = \frac{1}{n}\sum_{i=1}^{n} F_i$. To compute the empirical probabilities, the Weibull plotting position is generally used:

$$F(v_i) = \frac{i}{n+1} \tag{6}$$

where $i = 1,...,n$ is the rank for ascending ordered observed wind speeds. This formula is frequently used with *P-P* plots because it always gives an unbiased estimate of the empirical cumulative probabilities regardless of the underlying distribution being considered [31]. Another alternative is to use the Cunnane plotting position [102]: $F(\mathrm{v}_i) = \frac{i - 0.4}{n + 0.2}$.

2.2.2. R^2_{QQ}

R_{QQ}^2 is the coefficient of determination associated with the *Q*-*Q* plot defined by the predicted wind speed quantiles versus the observed wind speeds. An example of a *Q*-*Q* plot is given in Fig. 1b. The *i*th predicted wind speed quantile $\hat{v}_i$ is given by $\hat{v}_i = F^{-1}(F_i)$, where $F^{-1}(x)$ is the inverse function of the theoretical cdf and F_i is the empirical probability of the *i*th observed wind speed. R_{QQ}^2 is computed as follows:

$$R_{QQ}^2 = 1 - \frac{\sum_{i=1}^{n} (v_i - \hat{v}_i)^2}{\sum_{i=1}^{n} (v_i - \bar{v})^2} \qquad (7)$$

where v_i is the *i*th observed wind speed and $\bar{v} = \frac{1}{n} \sum_{i=1}^{n} v_i$.

2.2.3. $\boldsymbol{R_{F,c}^2}$

For the following two R^2 statistics, observed wind speed data are arranged in a relative frequency histogram having N class intervals. $R_{F,c}^2$ is the coefficient of determination measuring the fit between the theoretical cdf and the cumulative relative frequency histogram of wind speeds. It is similar to R_{PP}^2 but is based on a histogram approach. An example of a *P*-*P* plot with histogram is given in Fig. 1c. $R_{F,c}^2$ is computed as follows:

$$R_{F,c}^2 = 1 - \frac{\sum_{i=1}^{N} (F_i - \hat{F}_j)^2}{\sum_{i=1}^{N} (F_i - \bar{F})^2} \qquad (8)$$

where $\hat{F}_i$ is the predicted cumulative probability at the *i*th class interval, F_i is the cumulative probability of relative frequencies at the *i*th class interval and $\bar{F} = \frac{1}{N} \sum_{i=1}^{N} F_i$.

2.2.4 $R_{p,c}^2$

$R_{p,c}^2$ is the coefficient of determination measuring the fit between the predicted probabilities at the class intervals obtained with the theoretical pdf and the relative frequencies of the histogram of wind speed data. An example of a graph representing the relation between these theoretical and observed probabilities is given in Fig. 1d. $R_{p,c}^2$ is computed as follows:

$$R_{p,c}^2 = 1 - \frac{\sum_{i=1}^{N} (p_i - \hat{p}_i)^2}{\sum_{i=1}^{N} (p_i - \bar{p})^2} \tag{9}$$

where $\hat{p}_i = F(v_i) - F(v_{i-1})$ is the estimated probability at the *i*th class interval, v_{i-1} and v_i are the lower and upper limits of the *i*th class interval, p_i is the relative frequency at the *i*th class interval and $\bar{p} = \frac{1}{N} \sum_{i=1}^{N} p_i$.

2.2.5. Adjusted R^2

In the R^2 statistics presented above, the parsimony is not considered. These statistics tend hence to favor more complex models, which use a larger number of parameters and provide increased flexibility. The adjusted R^2, denoted R_a^2, was developed to penalize the statistic for additional parameters. It is given by the following adjustment formula:

$$R_a^2 = 1 - (1 - R^2) \frac{N - 1}{N - d} \tag{10}$$

where R^2 is anyone of the R^2 statistics presented above, d is the number of parameters in the model and N is the wind speed sample size or the number of class intervals in the case of statistics based on the histogram approach.

2.3. Root mean square error (RMSE)

The RMSE evaluates the difference between the observed and predicted values. It is generally used either with predicted wind speed values (i.e., $\mathrm{RMSE}_v = \left[\sum_{i=1}^{n} (v_i - \hat{v}_i)^2 / n\right]^{1/2}$), or with predicted relative frequencies of the histogram of wind speed data, (i.e., $\mathrm{RMSE}_p = \left[\sum_{i=1}^{N} (p_i - \hat{p}_i)^2 / \mathrm{N}\right]^{1/2}$). RMSE_v is associated with the *Q*-*Q* plot in Fig. 1b and RMSE_p is associated with the graph in Fig. 1d. It is important to mention that the RMSE is considered as an important performance index since it combines both the dispersion and the bias. It can be shown for instance in the case of RMSE_v (see [103]) that we have: $\mathrm{RMSE}_v^2 = \frac{(n-1)}{n}\mathrm{STD}_v^2 + bias_v^2$ where STD_v is the standard error of the data and $bias_v$ is the bias of predicted wind speed values.

2.4. Chi-square test statistic (χ^2)

The Chi-Square test accepts or rejects the null hypothesis that the observed sample distribution is consistent with a given theoretical distribution. The test statistic is first computed and a critical value for the test is found at a given significance level. In the context of the assessment of model distributions for wind speed data, the statistical value of the test is often used to compare the goodness-of-fit of several theoretical distributions. To compute the Chi-Square test statistic, the sample is arranged in a frequency histogram having N class intervals. The Chi-Square test statistic is given by:

$$\chi^2 = \sum_{i=1}^{N} \frac{\left(O_i - E_i\right)^2}{E_i} \tag{11}$$

where O_i is the observed frequency in the ith class interval and E_i is the expected frequency in the ith class interval. E_i is given by $F(v_i) - F(v_{i-1})$ where v_{i-1} and v_i are the lower and upper limits of the ith class interval. A minimum expected frequency is usually required for each class interval as an expected frequency that is too small for a given class interval will have too much weight. When an expected frequency of a class interval is too small, it is usually combined with the adjacent class interval.

2.5. Kolmogorov-Smirnov (KS) and Anderson-Darling (AD) test statistics

The KS and AD tests are also used to judge the adequacy of a given theoretical distribution for a given set of observed wind speed data. Like the Chi-Square test in the context of the assessment of model distributions to wind speed data, the values of the statistics of these tests are often used to compare the goodness-of-fit of several theoretical distributions to the observed data. Both KS and AD statistics compare the cdf of the theoretical distribution with the empirical cumulative probability distribution of wind speed data. Fig. 2 illustrates an example of both cumulative distributions sketched together on the same plot. The KS test computes the largest difference between the predicted and the observed distribution. The KS-test statistic is given by:

$$D = \max_{1 \le i \le n} \left| F_i - \hat{F}_i \right|. \tag{12}$$

where $\hat{F}_i$ is the ith predicted cumulative probability from the theoretical cdf and F_i is the empirical probability of the ith observed wind speed. The AD [104] test statistic is defined by the following equation:

$$A = n\int_{-\infty}^{\infty}\left[F(x)-\hat{F}(x)\right]^2 \psi(F(x))dF(x) \qquad (13)$$

where $\psi(\mathrm{x}) = \left[\hat{F}(x)(1-\hat{F}(x))\right]^{-1}$ is a nonnegative weight function. Eq. (13) can be rewritten for a finite data sample as:

$$A = \left\{-n-\sum_{i=1}^{n}\frac{2i-1}{n}\left[\ln(\hat{F}_i)+\ln(1-\hat{F}_{n-i+1})\right]\right\}. \qquad (14)$$

Because of the weight function, the AD test gives more weight to the tails of the distribution than the KS test.

2.6. Advantages and disadvantages of the different methods

The methods presented above have different advantages and disadvantages. R^2_{PP}, $R^2_{F,c}$, KS and AD are related to the *P-P* plot. They are hence more sensitive to the middle part of the wind speed distribution where the gradient of the cumulative distribution function is the largest [105]. Fig. 3a presents a graph of a hypothetical cdf showing the effect of small differences in wind speed (Δv) on the probabilities *p*. It can be seen that Δv in the middle part of the distribution produces a larger variation in *p* than in the right tail. Because of the weight function involved in the definition of the AD test, it is more sensitive to the tails of the distribution than KS.

R^2_{QQ} is related to the *Q-Q* plot. It is hence more sensitive to the tails of the distribution where the gradient of the inverse cumulative distribution function is largest [105]. Fig. 3b presents a graph of a hypothetical inverse cdf showing the effect of small differences in the percentile (Δp) on the wind speed quantiles *v*. It can be seen that Δp in the right tail of the distribution produces a larger variation in the quantiles than in the middle part.

The use of *P-P* plots is often preferred over the use of *Q-Q* plots because the Weibull plotting position provides an unbiased estimate of the observed cumulative probabilities for the *P-P* plot independently of the theoretical distribution considered [31, 32]. Ln *L*, AIC and BIC are also more sensitive to the tails of the distributions. Indeed, the definition of these criteria includes the sum of the logarithmically transformed densities of the observed wind speeds, and the magnitude of the logarithmically transformed density is larger in the tails than in the middle part of the distribution.

$R^2_{p,c}$, RMSE_p and χ^2 are associated with probabilities in class intervals. Because χ^2 is a measure of the relative error in class intervals, it is more sensitive to the tails of the distribution where the expected frequencies are small than $R^2_{p,c}$ and RMSE_p.

The majority of the criteria discussed above do not take into account the parsimony of the models. AIC, BIC and R^2_a, on the other hand, penalize models that have a larger number of parameters. The use of the adjusted R^2 (R^2_a) is more relevant when the histogram approach is adopted ($R^2_{F,c}$, $R^2_{p,c}$). On the other hand, when no histograms are defined and the wind speed data is used directly (R^2_{PP}, R^2_{QQ}), the adjusted R^2 is very similar to the conventional R^2 because of the large sample size usually available in wind speed analysis. Indeed, Eq. (10) shows that when N is very large compared to d, we have $R_a^2 \approx R^2$ and the adjustment due to the number of parameters is not significant.

Criteria that use the histogram approach (χ^2, $R_{F,c}^2$, $R_{p,c}^2$ and RMSE_p) have the advantage of being less affected by individual observations. However, the results depend on the subjective choice of class intervals.

It is important to note that χ^2, KS and AD are commonly used in practice to evaluate if a given theoretical distribution represents the parent distribution of a given data set. This is due to the fact that these represent statistical tests with explicitly defined test critical values. The critical values for χ^2 and AD depend on the theoretical distribution, while the critical value is independent of the theoretical distribution for KS.

Finally, the values of the criteria R^2, χ^2, KS and AD are on scales that are independent of the sample considered and thus these criteria can be used to compare the fit of different samples (stations). This is not possible with criteria such as AIC or RMSE, as their values will differ significantly from one data sample to another. These criteria can only be used to compare the fit of different models for the same data set.

2.7. Wind power error

Celik [4] points out that in the field of wind engineering, wind speed distribution functions are ultimately used to correctly model the wind power density. Therefore, the most important criterion for the suitability of a possible wind speed distribution function should be based on how successful it is in predicting the observed wind power density. For a given theoretical pdf $f(v)$ fitted on the wind speed data, the resulting wind power density distribution is given by:

$$P(v) = \frac{1}{2}\rho v^3 f(v) \qquad (15)$$

where ρ is the air density. The fit is often evaluated visually by plotting the estimated power density distributions of the candidate pdfs along with the wind power density histogram obtained from the observed wind speed data. The R^2, χ^2, standard deviation and RMSE are commonly used as objective criteria to measure the goodness-of-fit in these graphs [4, 15, 17, 21, 51, 66, 68, 69].

Another popular approach involves comparing the mean wind power output [1, 13, 26, 31, 32, 65] (or the wind energy output [5, 21]) generated from the theoretical pdf with the mean wind power output calculated from the observed wind speed data. The mean wind power density for the theoretical pdf $f(v)$ is obtained by integrating Eq. (15):

$$\hat{\bar{P}}_0 = \frac{1}{2}\int_0^\infty \rho v^3 f(v) dv \ . \qquad (16)$$

The mean wind power density calculated from the observed wind speed data is given by:

$$\bar{P}_0 = \frac{1}{2}\rho \overline{v^3}. \qquad (17)$$

Alternatively, a specific wind turbine is sometimes considered for the computation of the power output. In that case the mean wind turbine power from the theoretical pdf and from the observed wind speed data are given respectively by:

$$\hat{\bar{P}}_w = \int_0^\infty P_w(v) f(v) dv \ , \qquad (18)$$

$$\bar{P}_w = \frac{1}{n}\sum_{i=1}^{n} P_w(v_i), \tag{19}$$

where $P_w(v)$ is the power curve of the wind turbine. The difference between the theoretical power output and observed power output is often represented by the relative percent error:

$$\varepsilon = \left| \frac{\hat{\bar{P}} - \bar{P}}{\bar{P}} \right| \times 100, \tag{20}$$

where $\bar{P} = \bar{P}_0(\bar{P}_w)$ and $\hat{\bar{P}} = \hat{\bar{P}}_0(\hat{\bar{P}}_w)$.

3 Theoretical background on moment and L-moment ratio diagrams

In the following, we present the mathematical background of conventional moment ratio diagrams and L-moment ratio diagrams respectively.

3.1 Moment ratio diagram

Let us define a random variable *X*. The *r*th central moment of *X* is given by

$$\mu_r = E(X - \mu)^r, \qquad r = 2, 3, \ldots, \tag{21}$$

where $\mu = E(X)$ is the mean of *X*. The *r*th moment ratio for *r* higher than 2 is defined by

$$C_r = \frac{\mu_r}{\mu_2^{r/2}}\ . \tag{22}$$

The 3rd and 4th moment ratios, also defined respectively as the coefficient of skewness (C_S) and the coefficient of kurtosis (C_K), are then

$$C_3 = C_S = \frac{\mu_3}{\mu_2^{3/2}}, \tag{23}$$

$$C_4 = C_K = \frac{\mu_4}{\mu_2^{2}}. \tag{24}$$

Moments are often computed from a data sample. Let us define $x_1, x_2, ..., x_n$, a data sample of size *n*. The *r*th sample central moments are

$$m_r = n^{-1}\sum_{i=1}^{n}(x_i - \bar{x})^r, \qquad r = 2,3,..., \tag{25}$$

where $\bar{x} = n^{-1}\sum_{i=1}^{n} x_i$ is the sample mean. Sample estimators of the coefficient of skewness and the coefficient of kurtosis are then respectively

$$\hat{C}_S = \frac{m_3}{m_2^{3/2}}, \tag{26}$$

$$\hat{C}_K = \frac{m_4}{m_2^{2}}. \tag{27}$$

Traditionally, moment ratio diagrams represent on a graph every possible value of β_1 in terms of β_2 where $\beta_1 = C_S^2$ and $\beta_2 = C_K$. Two-parameter distributions with a location parameter and a scale parameter plot as a single point in the moment ratio diagram. Two and three-parameter distributions with one shape parameter plot as a curve. Three and four-parameter distributions with two or more shape parameters cover a whole area in the diagram. For all distributions, it can be shown that the condition $\beta_2 - \beta_1 - 1 \geq 0$ must be satisfied and thus an impossible region exists in the diagram graph [106].

Moment ratio diagrams can be used to select a pdf to model a given data sample. For this, the sample estimates $\hat{\beta}_1 = \hat{C}_S^2$ and $\hat{\beta}_2 = \hat{C}_K$ are computed from the data sample and the point $(\hat{\beta}_1, \hat{\beta}_2)$ representing the sample is plotted in the moment ratio diagram. The pdf is then selected by comparing the position of this point with the theoretical pdfs represented on the moment ratio diagram.

3.2 L-moment ratio diagram

L-moments, introduced by Hosking [81], are linear combinations of probability weighted moments (PWM). They are analogous to the conventional moments. Let us define a random variable X with a cumulative distribution function $F(X)$ and a quantile function $x(u)$. PWMs were defined in Greenwood et al. [107] by the following expression:

$$M_{p,r,s} = E[\mathrm{X}^p \{\mathrm{F(X)}\}^r \{1 - \mathrm{F(X)}^S\}] . \tag{28}$$

A useful special case of the PWM is $B_r = M_{1,\mathrm{r},0}$ given by

$$B_r = E[X\{F(X)\}^r] = \int_0^1 x(u) u^r du . \tag{29}$$

The L-moments of X are defined in Hosking [81] to be the quantities

$$\lambda_{r+1} = \sum_{k=0}^{r} p_{r,k}^* B_k , \tag{30}$$

where

$$p^*_{r,k} = (-1)^{r-k}\binom{r}{k}\binom{r+k}{k}. \tag{31}$$

The dimensionless L-moment ratios, L-variation, L-skewness and L-kurtosis, are respectively defined by

$$\begin{aligned} \tau_2 &= \lambda_2 / \lambda_1 \\ \tau_3 &= \lambda_3 / \lambda_2 \,. \\ \tau_4 &= \lambda_4 / \lambda_2 \end{aligned} \tag{32}$$

L-moments possess an important property which makes them attractive for distribution fitting to sample data and for the assessment of the goodness-of-fit: If the mean of the distribution exists, then all L-moments exist and the L-moments uniquely define the distribution [79, 81]. τ_4 is usually plotted against τ_3 in L-moment ratio diagrams. As with conventional moment ratio diagrams, the number of shape parameters determines if the pdf plots as a point, a curve or an area in the diagram.

L-moments are often estimated from a finite sample. Let us define $x_{1:n} \le x_{2:n} \le \cdots \le x_{n:\mathrm{n}}$, an ordered sample of size *n*. An unbiased estimator of the *r*th probability weighted moment B_r is

$$b_r = n^{-1}\binom{n-1}{r}^{-1}\sum_{j=r+1}^{n}\binom{j-1}{r}x_{j:n}\,. \tag{33}$$

The sample L-moments are defined by

$$\ell_{r+1} = \sum_{k=0}^{r} p^*_{r,k} b_k\,, \qquad r = 0,1,\ldots,n-1. \tag{34}$$

Analogously to Eq. (32), the sample L-moment ratios are defined by

$$\begin{aligned} t_2 &= \ell_2 / \ell_1 \\ t_3 &= \ell_3 / \ell_2 \, . \\ t_4 &= \ell_4 / \ell_2 \end{aligned} \tag{35}$$

4 Representation of probability distribution functions in moment ratio diagrams

This section presents the methodology used to represent the selected pdfs in the moment and L-moment ratio diagrams. Table 1 presents the pdfs of all selected distributions with their domain and number of parameters. For several pdfs, explicit expressions of β_2 as function of β_1 or τ_4 as function of τ_3 are available in the literature in the form of polynomial approximations. These expressions are then directly used to represent the points or curves. The expressions relating β_1 and β_2 on one side, and τ_4 and τ_3 on the other sides, for the distributions EV1, GEV, G, P3, LN2 and LN3 are given in Rao and Hamed [80] and Hosking and Wallis [79] respectively. They also give the explicit expression for the bounds delineating the impossible regions. G and P3 on one side and LN2 and LN3 on the other side have the same 3rd and 4th moment ratios, and are hence represented by the same curve on the diagrams. The curve of the W2 distribution can be obtained using the fact that τ_3 and τ_4 (or C_S and C_K) for the W2 equal respectively $-\tau_3$ and τ_4 (or $-C_S$ and C_K) for the GEV.

For pdfs that define areas (GG, LP3 and KAP), we are interested in defining the curves that define the bounds of the areas. Analytical expressions of these curves are not available. The relations between moments and distribution parameters are hence used and the numerical method described below is applied. For a given pdf with three or four-parameters, let us define two shape parameters *h* and *k*, and a position parameter μ and/or a scale parameter α. The 2nd and 3rd moment ratios are independent of μ and α, and are hence given arbitrary values. Parameters *h* and *k* are varied over a large range within the feasibility domain of the given pdf with small intervals ($h = h_1, h_2, \ldots, h_n; k = k_1, k_2, \ldots, k_m$). For each possible pair (h_i, k_j), where h_i and k_j are the *i*th and *j*th shape parameters, the corresponding pairs of moment ratios ($\beta_{1,i,j}, \beta_{2,i,j}$) and ($\tau_{3,i,j}, \tau_{4,i,j}$) are obtained and are plotted on the moment ratio diagram and L-moment ratio diagram respectively. This way, the contours of the regions defined by these points are found. For most distributions, the shape parameters are unbound either in the positive or the negative direction, and sometimes in both directions. This makes it impossible to explore the entire feasibility domain of each parameter. However, for a given parameter, as its value becomes very large or very small, points obtained in the moment ratio diagrams always converge to a limit case. By using ranges with sufficiently extreme values for parameters in unbound directions, an approximate area that accurately describes the feasible region is obtained.

The application of this method requires the use of the expressions relating moments and L-moments with distribution parameters. Bobée et al. [78] derived the expressions relating β_1 and β_2 with the parameters of the GG and LP3 from the existing relation between noncentral moments μ'_r and distribution parameters and from the relation between central moments μ_r and noncentral moments μ'_r given in Kendall and Stuart [108]. This same approach is applied here for the KAP distribution where the relation between μ'_r and the distribution parameters are found in Winchester [109]. The expressions of L-moment ratios τ_3 and τ_4 as functions of the distribution parameters of the KAP are given in Hosking and Wallis [79]. However, explicit expressions of L-moments in terms of the distribution parameters of the GG and LP3 are not available. In this case, the values of B_r in Eq. (29) are solved by numerical integration. Estimated B_1, B_2 and B_3 are then put in Eq. (30) to obtain λ_2, λ_3 and λ_4 and subsequently τ_3 and τ_4.

Figs. 4 and 5 present the moment ratio diagram and the L-moment ratio diagram obtained for the selected pdfs of this study. These diagrams allow to analyze the flexibility of the different pdfs: a pdf that can take on many different values of skewness and kurtosis is more flexible in terms of shape of the distribution [77]. EV1 plots as a single point. Without any shape parameter, it has no flexibility. It is a special case of the GEV. The GEV, W2-W3, G-P3 and LN2-LN3 distributions having one shape parameter plot as lines. They are equivalent around zero skewness. G-P3 and W2-W3 are special cases of the GG. The location parameter μ of LN2-LN3 also acts as a shape parameter because of the logarithmic transformation on *x*. GG, LP3 and KAP plot as a whole area. KAP is the most flexible followed by LP3 and GG. GG and KAP have 2 shape parameters. The location parameter μ of LP3 also acts as a shape parameter because of the logarithmic transformation on *x*.

5. Case study

The United Arab Emirates (UAE) is located in the south-eastern part of the Arabian Peninsula. It is bordered by the Persian Gulf in the north, the Arabian Sea and Oman in the east, and Saudi Arabia in the south and west. It lies approximately between 22°40’N and 26°N and between

51°E and 56°E. The total area of the UAE is about 83,600 km^2. It can be divided into three ecological areas: the northeastern mountainous area, the sandy/desert inland area and the marine coastal area. The desert covers 80% of the country. The climate of the UAE is arid with very high temperatures during summer. The coastal area has a hot and humid summer with temperatures and relative humidity reaching 46 °C and 100% respectively. During winter, temperatures are between 14 °C and 23 °C. The interior desert region has hot summers with temperatures rising to about 50 °C and cool winters during which the temperatures can fall to around 4 °C [110, 111].

The Wind speed data used in this study comes from 7 meteorological stations located throughout the UAE. Anemometers are at the 10 m height for all stations. Table 2 gives a description of the stations including geographical coordinates, altitude, period of record, and wind speed statistics including maximum, mean, median, standard deviation, coefficient of variation, coefficient of skewness and coefficient of kurtosis. Periods of record range from 11 months to 39 months. A map indicating the location of the stations is given in Fig. 6. The whole geographical region of the UAE is well represented by these stations: The stations of Sir Bani Yas Island, Al Mirfa and Masdar city are located near the coastline, the station of East of Jebel Haffet is located in the mountainous north-eastern region, the station of Al Aradh is location in the foothills and the stations of Al Wagan and Madinat Zayed are located inland. The inter-annual variability and the long term evolution of wind speed data in these stations was studied by Naizghi and Ouarda [112].

Wind speed data used in this study was collected by anemometers at 10-min intervals. Average hourly wind speed series, which is the most common time step used for characterizing short term wind speeds, were then computed from the 10-min wind speed series. The resulting hourly wind speed data can theoretically contain null values, as periods of calm can possibly last more than one hour. For pdfs having a null probability of observing null wind speed, this would make it impossible to estimate the distribution parameters with some methods. Therefore, any null values are removed from the hourly data series of this study. The impact of removing null values was checked to be insignificant as observed percentages of calms in the hourly time series are marginally low.

6. Results

Sample moments and sample L-moments were computed for each wind speed series with Eqs. (26) and (27), and Eq. (32) respectively. Wind speed samples were plotted in the moment ratio diagram and the L-moment ratio diagram. These diagrams are presented in Figs. 7 and 8 respectively. Each station is numbered according to its rank in Table 2. The analysis of the diagrams leads to the following conclusions about the suitability of the pdf to fit the stations sample data. The curve of the W2-W3 passes through the middle of the cloud of points defined by the samples. The G-P3, GEV and LN2-LN3 are located rather in the margin of the cloud of points and are consequently not suitable to fit wind speed data. This makes W2-W3 the most suitable pdf with one shape parameter for wind speed data in the UAE. However, some station samples, such as stations 4 and 6, might be located far from the curve of the W2-W3. Alternatively, all station samples are located within the regions bounded by GG, LP3 and KAP.

The selected pdfs were fitted to the wind speed data corresponding to all stations of this study. The methods used for the estimation of the parameters of each pdf are also listed in Table 1. For the majority of the distributions, the maximum likelihood method (ML) and/or the method of moments (MM) were used. For KAP, the method of L-moments (LM) was used instead of MM. The algorithm used for estimating the parameters with LM was proposed by Hosking [113]. For the LP3, the Generalized Method of Moments (GMM) [114, 115] is used.

Each candidate distribution/method (D/M), a combination of a distribution with an estimation method from Table 1, was fitted to the wind speed series presented in the case study. The following criteria of goodness-of-fit were then calculated: ln L, $R_{F,c}^2$, $R_{p,c}^2$, χ^2, KS and AD. For the coefficients of determination $R_{F,c}^2$ and $R_{p,c}^2$, the adjusted version is considered. Table 3 lists the 6 best pdfs based on the goodness-of-fit criteria. In Fig. 9, each criterion except ln L is presented with box plots representing the various D/Ms for all stations combined. For each distribution, the D/M with the method leading to the best fit is represented. LN2 leading to generally very poor fits was discarded from these box plots.

The conclusions obtained from the moment ratio diagrams are in general in agreement with those obtained with the analysis of goodness-of-fit criteria. According to $R_{F,c}^2$, KAP is by far the best pdf followed by GG and LP3. According to $R_{p,c}^2$, GG followed by KAP and LP3 are the best pdfs. GG, W3 and KAP are, in this order, the best pdfs with respect to the χ^2 statistic, while KAP, GG and LP3 are, in this order, the best pdfs with respect to the KS statistic. According to AD, KAP and LP3 are the best pdfs. Based on the ranks obtained in Table 3 for ln L, KAP is the best pdf followed in order by GG and W3. KAP is more flexible and is listed among the best D/Ms for all 7 stations while GG is not included among the best pdfs for the stations of Al Mirfa, East of Jebel Haffet and Madinat Zayed.

Box plots reveal that the W2 is the best two-parameter distribution and leads to better performances than several three-parameter distributions including the GEV, LN3 and P3.

According to most criteria, LP3 gives inferior fit than GG. This is surprising considering the location of the samples which are within the area covered by the pdf. This point will be further discussed below.

The relations between the location of individual stations on the moment and L-moment ratio diagrams and the results obtained with the goodness-of-fit criteria are investigated. The analysis of the conventional moment ratio diagram (Fig. 7) reveals the following: For Station 6, located far from all curves, KAP, GG and LP3, which are pdfs that define regions, are preferred with respect to all criteria. Furthermore, the clear outlier for P3/MM in the box plots of $R^2_{F,c}$ and $R^2_{p,c}$ corresponds to Station 6. Station 7 is close to the GEV curve in the diagram and this distribution received generally good ranks for this station. On the other hand, Station 4 is right on the G-P3 curve but these pdfs are not particularly higher ranked for this station.

In the L-moment ratio diagram (Fig. 8), the following can be observed: Stations 1, 2 and 7 are very close to the W2 curve. The ranks of the W2 or W3 for these stations are generally higher than those of the other stations. Station 6 is also located far from the curves of the pdfs in this diagram. Station 4 is located near the border of the region delineated by GG and LP3. This is in agreement with the goodness-of-fit criteria which indicate that the GG and LP3 do not perform very well for all criteria. Station 4 is also located very close to the curve of the GEV and the point corresponding to EV1. These pdfs perform much better for this station while they perform poorly for the others. Station 5, is located near the G-P3 curve. The goodness-of-fit criteria obtained for this station are generally excellent.

In Fig. 10, the wind speed frequency histograms corresponding to each station are presented. The pdfs of the W3/ML, GG/MM, LP3/GMM and KAP/LM are superimposed over these plots.

These plots allow to visualize and validate the fit obtained by the selected distributions. The distribution parameters of the selected pdfs for each station are presented in Table 4. The KAP distribution gives generally the best fit. In the case of station 1, no distribution was able to model the lower part of this particular shape of histogram. This distribution presents a bimodal behavior. This case illustrates the limitation of classical models in the presence of bimodality. W3 fails to model adequately the distribution of East of Jebel Haffet and Masdar City (4 and 6 respectively). Consistently, stations 4 and 6 are located far from the W2-W3 theoretical curve in the moment ratio diagrams. For East of Jebel Haffet and Madinat Zayed (stations 4 and 5 respectively), the pdfs of W3 displayed on the histograms underestimate the probability density in the part of the distribution with the higher frequencies. Consistently, the locations of these stations in the L-moment ratio diagram indicate that each sample data has a higher kurtosis than the theoretical distribution of W2-W3 for a given skewness. In the conventional moment ratio diagram, this consistency is not well observed as the location of station 5 indicates that the observed data for that station have a lower kurtosis than the theoretical distribution of W2-W3 for the same skewness.

These results indicate that the goodness-of-fit criteria are more consistent with the results obtained with the L-moment ratio diagram than with the conventional moment diagram. Indeed, the location of individual stations in the L-moment ratio diagram allows drawing more conclusions in agreement with the results obtained with the majority of the goodness-of-fit criteria. This is in agreement with previous studies in the field of hydro-meteorology, where the L-moment ratio diagram instead of the conventional moment ratio diagram was recommended. Hosking [81] suggested the use of the L-moment ratio diagram especially for small size samples because L-moment estimators are less biased than conventional moment estimates. Vogel and

Fennessey [99] found that conventional moment estimators are also biased for large samples from highly skewed distributions.

As presented in the literature review, the model distributions are also often evaluated for their ability to model the average wind power. A comparison of the model distributions is also presented herein using this criterion. The mean power density is computed using Eq. 17 and the mean power densities for the theoretical distributions are computed using Eq. 16. Table 5 presents the mean power density obtained for the observed data and from the theoretical distributions. The D/Ms that provide the best fits are LP3/GMM, P3/MM, GG/MM, GEV/MM, LN3/MM and KAP/LM. These results are somewhat different from those obtained with the other criteria. Indeed the GEV and LN3 distributions which lead to good results with the average wind power criterion did not lead to equivalent performances with the other criteria. Fig. 11 presents the wind power density frequency histogram for each station. Similarly to Fig. 10, the distributions for the W3/ML, GG/MM, LP3/GMM and KAP/LM are superimposed over these plots.

7. Conclusions and future work

In this study, a review of the various criteria used in the field of wind energy was presented, along with a discussion of their advantages and disadvantages. The methods of moment ratio and L-moment ratio diagrams were used for the assessment of pdfs to fit short term wind speed data samples. These methods, often used in hydro-meteorology, offer a viable alternative to goodness-of-fit tests and criteria commonly used for the analysis of wind speed data. Their main advantage is that they allow an easy comparison of the fit of several pdfs on a single diagram.

They are also easy to implement and the position of the time series on the diagrams are easily computed with the moment equations.

Diagrams for the conventional moment ratios and for the L-moment ratios were built for a selection of 11 pdfs. For most pdfs defining a curve, expressions of β_2 in terms of β_1 or τ_4 in terms of τ_3 are available in the literature. This allows a straightforward representation of curves in the moment ratio diagrams. However, for pdfs with two shape parameters (KAP, GG and LP3), an area is instead covered in the moment ratio diagrams and analytical expressions relating the moment ratios to the limits of the areas are generally not available in the literature. An easy numeric procedure is used to define the limits of these areas. Plotting the position of a given wind speed data set in these diagrams is instantaneous and provides more information than a goodness-of-fit criterion since it provides knowledge about such characteristics as the skewness and kurtosis of the station data set. These diagrams have also the advantage of allowing an easy comparison of the fit of several pdfs for several stations on a single diagram.

The method of moment ratio diagrams was applied here to a study case consisting of short term wind speed data recorded in the UAE. Moment ratio diagrams were used to evaluate the suitability of several pdfs to fit wind speed data. The conclusions based on the moment ratio diagrams are as follows: Compared to other pdfs having one shape parameter and thus defining a curve on the moment ratio diagram, W2 or W3 have the most central position with respect to sample coordinates and should be considered as the best choice among these pdfs. However, some samples could be located far from this curve. The pdfs with two shape parameters, GG, LP3 and KAP, cover an area that encompasses every sample. KAP is the most flexible distribution and hence its area covers the largest part of the diagrams.

Conclusions obtained with the diagrams were compared to results obtained with goodness-of-fit criteria. It was observed that a better agreement exists between the conclusions drawn from goodness-of-fit criteria and those from the L-moment ratio diagram, than those from the conventional moment ratio diagram. This is in agreement with the theoretical advantages of the L-moments and the results of the previous studies which concluded that L-moment ratio diagrams should be used instead of conventional moment ratio diagrams. It is concluded that these diagrams can represent a simple and efficient approach to be used in association with commonly known goodness-of-fit criteria.

Classical frequency analysis tools used in wind speed modeling are based on the hypothesis of temporal stationarity of the wind speed data. In reality, such assumption is not always met. A considerable amount of research dealt with the development of non-stationary frequency analysis procedures for hydro-climatic variables (see for instance [116, 117]). Future work should focus on the use of non-stationary frequency analysis techniques for the modeling of wind speed series in various regions around the globe. Moment ratio diagrams have never been used in the non-stationary context and can be adapted easily to analyze the temporal evolution of wind speed characteristics. It is possible for instance to study the evolution of the position of a given sample in the moment or L-moment ratio diagrams by considering a moving window through the data series.

Acknowledgements

The authors wish to thank Masdar Power for having supplied the wind speed data used in this study. The authors wish to express their appreciation to Dr. Mohamed Al-Nimr, Editor in Chief, Dr. Nesreen Ghaddar, Editor, and three anonymous reviewers for their invaluable comments and suggestions which helped considerably improve the quality of the paper.

Nomenclature

b_r	unbiased estimator of B_r
B_r	rth probability weighted moment where $M_{1,r,0}$
β_1	moment ratio C_S^2
β_2	moment ratio C_K
C_V	coefficient of variation
C_S	coefficient of skewness
C_K	coefficient of kurtosis
cdf	cumulative distribution function
χ^2	Chi-square test statistic
D/M	distribution/method
EV1	Gumbel or extreme value type I distribution
$f_{\hat{\theta}}(\,)$	probability density function with estimated parameters $\hat{\theta}$
$\hat{f}(\,)$	estimated probability density function
F_i	empirical probability for the ith wind speed observation
$\hat{F}_i$	estimated cumulative probability for the ith observation obtained with the theoretical cdf
$F(\,)$	cumulative distribution function
$F^{-1}(\,)$	inverse of a given cumulative distribution function

G	Gamma distribution
GEV	generalized extreme value distribution
GG	generalized Gamma distribution
GMM	generalized method of moment
KAP	Kappa distribution
KS	Kolmogorov-Smirnov test statistic
ℓ_{r+1}	sample *r*th L-moment
LM	Method of L-moments
LN2	2-parameter Lognormal distribution
LN3	3-parameter Lognormal distribution
LP3	Log-Pearson type III
ML	maximum likelihood
MM	method of moments
μ_r	*r*th central moment
n	number of wind speed observations in a series of wind speed observations
N	number of bins in a histogram of wind speed data
p_i	the relative frequency at the *i*th class interval
$\hat{p}_i$	the estimated probability at the *i*th class interval
$\hat{\bar{P}}_0$	mean wind power density for the theoretical pdf $f(v)$
$\bar{P}_0$	mean wind power density calculated from the observed wind speed data

$\hat{\bar{P}}_w$	mean wind turbine power from the theoretical pdf $f(v)$
$\bar{P}_w$	mean wind turbine power from the observed wind speed data
P3	Pearson type III distribution
pdf	probability density function
R^2	coefficient of determination
R_a^2	adjusted R^2
R_{PP}^2	coefficient of determination giving the degree of fit between the theoretical cdf and the empirical cumulative probabilities of wind speed data.
R_{QQ}^2	coefficient of determination giving the degree of fit between the theoretical wind speed quantiles and the wind speed data.
RMSE	root mean square error
m_r	rth sample central moment
$M_{p,r,s}$	probability weighted moment of order p, r, s
τ_r	rth L-moment ratio
t_r	rth sample L-moments ratio
v_i	the ith observation of the wind speed series
$\hat{v}_i$	predicted wind speed for the ith observation
W2	2-parameter Weibull distribution
W3	3-parameter Weibull distribution

References

[1] Akpinar EK, Akpinar S. A statistical analysis of wind speed data used in installation of wind energy conversion systems. Energy Convers Manage. 2005;46:515-32.

[2] Auwera L, Meyer F, Malet L. The use of the Weibull three-parameter model for estimating mean power densities. J Appl Meteor. 1980;19:819-25.

[3] Ayodele TR, Jimoh AA, Munda JL, Agee JT. Wind distribution and capacity factor estimation for wind turbines in the coastal region of South Africa. Energy Convers Manage. 2012;64:614-25.

[4] Celik AN. Assessing the suitability of wind speed probability distribution functions based on wind power density. Renew Energ. 2003;28:1563-74.

[5] Celik AN. Energy output estimation for small-scale wind power generators using Weibull-representative wind data. J Wind Eng Ind Aerod. 2003;91:693-707.

[6] Fichaux N, Ranchin T. Evaluating the offshore wind potential. A combined approach using remote sensing and statistical methods. Geoscience and Remote Sensing Symposium, 2003 IGARSS '03 Proceedings 2003 IEEE International2003. p. 2703-5.

[7] Hennessey JP. Some aspects of wind power statistics. J Appl Meteor. 1977;16:119-28.

[8] Hundecha Y, St-Hilaire A, Ouarda TBMJ, El Adlouni S, Gachon P. A Nonstationary Extreme Value Analysis for the Assessment of Changes in Extreme Annual Wind Speed over the Gulf of St. Lawrence, Canada. Journal of Applied Meteorology and Climatology. 2008;47:2745-59.

[9] Justus CG, Hargraves WR, Yalcin A. Nationwide assessment of potential output from wind-powered generators. J Appl Meteor. 1976;15:673-8.

[10] Mirhosseini M, Sharifi F, Sedaghat A. Assessing the wind energy potential locations in province of Semnan in Iran. Renew Sust Energ Rev. 2011;15:449-59.

[11] Petković D, Shamshirband S, Anuar NB, Saboohi H, Abdul Wahab AW, Protić M, et al. An appraisal of wind speed distribution prediction by soft computing methodologies: A comparative study. Energy Convers Manage. 2014;84:133-9.

[12] Solyali D, Altunç M, Tolun S, Aslan Z. Wind resource assessment of Northern Cyprus. Renew Sust Energ Rev. 2016;55:180-7.

[13] Chang TP. Estimation of wind energy potential using different probability density functions. Appl Energy. 2011;88:1848-56.

[14] Yip CMA, Gunturu UB, Stenchikov GL. Wind resource characterization in the Arabian Peninsula. Appl Energy. 2016;164:826-36.

[15] Li M, Li X. Investigation of wind characteristics and assessment of wind energy potential for Waterloo region, Canada. Energy Convers Manage. 2005;46:3014-33.

[16] Akdağ SA, Dinler A. A new method to estimate Weibull parameters for wind energy applications. Energy Convers Manage. 2009;50:1761-6.

[17] Carta JA, Ramirez P, Velazquez S. A review of wind speed probability distributions used in wind energy analysis Case studies in the Canary Islands. Renew Sust Energ Rev. 2009;13:933-55.

[18] Ahmed Shata AS, Hanitsch R. Evaluation of wind energy potential and electricity generation on the coast of Mediterranean Sea in Egypt. Renew Energ. 2006;31:1183-202.

[19] Bataineh KM, Dalalah D. Assessment of wind energy potential for selected areas in Jordan. Renew Energ. 2013;59:75-81.

[20] Carrasco-Díaz M, Rivas D, Orozco-Contreras M, Sánchez-Montante O. An assessment of wind power potential along the coast of Tamaulipas, northeastern Mexico. Renew Energ. 2015;78:295-305.

[21] Celik AN. On the distributional parameters used in assessment of the suitability of wind speed probability density functions. Energy Convers Manage. 2004;45:1735-47.

[22] Kiss P, Jánosi IM. Comprehensive empirical analysis of ERA-40 surface wind speed distribution over Europe. Energy Convers Manage. 2008;49:2142-51.

[23] Kucukali S, Dinçkal Ç. Wind energy resource assessment of Izmit in the West Black Sea Coastal Region of Turkey. Renew Sust Energ Rev. 2014;30:790-5.
[24] Tizpar A, Satkin M, Roshan MB, Armoudli Y. Wind resource assessment and wind power potential of Mil-E Nader region in Sistan and Baluchestan Province, Iran – Part 1: Annual energy estimation. Energy Convers Manage. 2014;79:273-80.
[25] Akpinar EK, Akpinar S. An assessment on seasonal analysis of wind energy characteristics and wind turbine characteristics. Energy Convers Manage. 2005;46:1848-67.
[26] Carta JA, Ramirez P, Velazquez S. Influence of the level of fit of a density probability function to wind-speed data on the WECS mean power output estimation. Energy Convers Manage. 2008;49:2647-55.
[27] Ouarda TBMJ, Charron C, Shin JY, Marpu PR, Al-Mandoos AH, Al-Tamimi MH, et al. Probability distributions of wind speed in the UAE. Energy Convers Manage. 2015;93:414-34.
[28] Shin J-Y, Ouarda TBMJ, Lee T. Heterogeneous mixture distributions for modeling wind speed, application to the UAE. Renew Energ. 2016;91:40-52.
[29] Lo Brano V, Orioli A, Ciulla G, Culotta S. Quality of wind speed fitting distributions for the urban area of Palermo, Italy. Renew Energ. 2011;36:1026-39.
[30] Masseran N, Razali AM, Ibrahim K. An analysis of wind power density derived from several wind speed density functions: The regional assessment on wind power in Malaysia. Renew Sust Energ Rev. 2012;16:6476-87.
[31] Morgan EC, Lackner M, Vogel RM, Baise LG. Probability distributions for offshore wind speeds. Energy Convers Manage. 2011;52:15-26.
[32] Soukissian T. Use of multi-parameter distributions for offshore wind speed modeling: The Johnson SB distribution. Appl Energy. 2013;111:982-1000.
[33] Zhou JY, Erdem E, Li G, Shi J. Comprehensive evaluation of wind speed distribution models: A case study for North Dakota sites. Energy Convers Manage. 2010;51:1449-58.
[34] Mert İ, Karakuş C. A statistical analysis of wind speed data using Burr, generalized gamma, and Weibull distributions in Antakya, Turkey. Turk J Elec Eng & Comp Sci. 2015;23:1571-86.
[35] Wang J, Hu J, Ma K. Wind speed probability distribution estimation and wind energy assessment. Renew Sust Energ Rev. 2016;60:881-99.
[36] Wu J, Wang J, Chi D. Wind energy potential assessment for the site of Inner Mongolia in China. Renew Sust Energ Rev. 2013;21:215-28.
[37] Dong Y, Wang J, Jiang H, Shi X. Intelligent optimized wind resource assessment and wind turbines selection in Huitengxile of Inner Mongolia, China. Appl Energy. 2013;109:239-53.
[38] Masseran N. Evaluating wind power density models and their statistical properties. Energy. 2015;84:533-41.
[39] Teyabeen AA. Statistical analysis of wind speed data. Renewable Energy Congress (IREC), 2015 6th International2015. p. 1-6.
[40] Bizrah A, AlMuhaini M. Modeling wind speed using probability distribution function, Markov and ARMA models. Power & Energy Society General Meeting, 2015 IEEE2015. p. 1-5.
[41] Masseran N, Razali AM, Ibrahim K, Latif MT. Fitting a mixture of von Mises distributions in order to model data on wind direction in Peninsular Malaysia. Energy Convers Manage. 2013;72:94-102.
[42] Qin X, Zhang J-s, Yan X-d. Two Improved Mixture Weibull Models for the Analysis of Wind Speed Data. Journal of Applied Meteorology and Climatology. 2012;51:1321-32.
[43] Akpinar S, Akpinar EK. Estimation of wind energy potential using finite mixture distribution models. Energy Convers Manage. 2009;50:877-84.
[44] Carta JA, Ramírez P, Bueno C. A joint probability density function of wind speed and direction for wind energy analysis. Energy Convers Manage. 2008;49:1309-20.
[45] Carta JA, Bueno C, Ramírez P. Statistical modelling of directional wind speeds using mixtures of von Mises distributions: Case study. Energy Convers Manage. 2008;49:897-907.
[46] Carta JA, Ramírez P. Use of finite mixture distribution models in the analysis of wind energy in the Canarian Archipelago. Energy Convers Manage. 2007;48:281-91.

[47] Jaramillo OA, Borja MA. Wind speed analysis in La Ventosa, Mexico: a bimodal probability distribution case. Renew Energ. 2004;29:1613-30.
[48] Kollu R, Rayapudi SR, Narasimham S, Pakkurthi KM. Mixture probability distribution functions to model wind speed distributions. International Journal of Energy and Environmental Engineering. 2012;3:1-10.
[49] Li M, Li X. MEP-type distribution function: a better alternative to Weibull function for wind speed distributions. Renew Energ. 2005;30:1221-40.
[50] Ramirez P, Carta JA. The use of wind probability distributions derived from the maximum entropy principle in the analysis of wind energy. A case study. Energy Convers Manage. 2006;47:2564-77.
[51] Akpinar S, Kavak Akpinar E. Wind energy analysis based on maximum entropy principle (MEP)-type distribution function. Energy Convers Manage. 2007;48:1140-9.
[52] Zhang H, Yu Y-J, Liu Z-Y. Study on the Maximum Entropy Principle applied to the annual wind speed probability distribution: A case study for observations of intertidal zone anemometer towers of Rudong in East China Sea. Appl Energy. 2014;114:931-8.
[53] Qin ZL, Li WY, Xiong XF. Estimating wind speed probability distribution using kernel density method. Electric Power Systems Research. 2011;81:2139-46.
[54] Zhang J, Chowdhury S, Messac A, Castillo L. A Multivariate and Multimodal Wind Distribution model. Renew Energ. 2013;51:436-47.
[55] Xu X, Yan Z, Xu S. Estimating wind speed probability distribution by diffusion-based kernel density method. Electric Power Systems Research. 2015;121:28-37.
[56] Usta I, Kantar YM. Analysis of some flexible families of distributions for estimation of wind speed distributions. Appl Energy. 2012;89:355-67.
[57] Conradsen K, Nielsen LB, Prahm LP. Review of Weibull Statistics for Estimation of Wind Speed Distributions. J Clim Appl Meteorol. 1984;23:1173-83.
[58] Garcia A, Torres JL, Prieto E, De Francisco A. Fitting wind speed distributions: A case study. Sol Energy. 1998;62:139-44.
[59] Bagiorgas HS, Mihalakakou G, Rehman S, Al-Hadhrami LM. Offshore wind speed and wind power characteristics for ten locations in Aegean and Ionian Seas. J Earth Syst Sci. 2012;121:975-87.
[60] Andrade CFd, Maia Neto HF, Costa Rocha PA, Vieira da Silva ME. An efficiency comparison of numerical methods for determining Weibull parameters for wind energy applications: A new approach applied to the northeast region of Brazil. Energy Convers Manage. 2014;86:801-8.
[61] Kantar YM, Usta I. Analysis of the upper-truncated Weibull distribution for wind speed. Energy Convers Manage. 2015;96:81-8.
[62] Pishgar-Komleh SH, Keyhani A, Sefeedpari P. Wind speed and power density analysis based on Weibull and Rayleigh distributions (a case study: Firouzkooh county of Iran). Renew Sust Energ Rev. 2015;42:313-22.
[63] Justus CG, Hargraves WR, Mikhail A, Graber D. Methods for Estimating Wind Speed Frequency Distributions. J Appl Meteor. 1978;17:350-3.
[64] Seguro JV, Lambert TW. Modern estimation of the parameters of the Weibull wind speed distribution for wind energy analysis. J Wind Eng Ind Aerod. 2000;85:75-84.
[65] Zhou Y, Smith SJ. Spatial and temporal patterns of global onshore wind speed distribution. Environmental Research Letters. 2013;8:034029.
[66] Chellali F, Khellaf A, Belouchrani A, Khanniche R. A comparison between wind speed distributions derived from the maximum entropy principle and Weibull distribution. Case of study; six regions of Algeria. Renew Sust Energ Rev. 2012;16:379-85.
[67] Kotroni V, Lagouvardos K, Lykoudis S. High-resolution model-based wind atlas for Greece. Renew Sust Energ Rev. 2014;30:479-89.
[68] Safari B. Modeling wind speed and wind power distributions in Rwanda. Renew Sust Energ Rev. 2011;15:925-35.
[69] Chang TP. Performance comparison of six numerical methods in estimating Weibull parameters for wind energy application. Appl Energy. 2011;88:272-82.

[70] Saleh H, Abou El-Azm Aly A, Abdel-Hady S. Assessment of different methods used to estimate Weibull distribution parameters for wind speed in Zafarana wind farm, Suez Gulf, Egypt. Energy. 2012;44:710-9.
[71] Zolfaghari S, Riahy GH, Abedi M. A new method to adequate assessment of wind farms' power output. Energy Convers Manage. 2015;103:585-604.
[72] Gökçek M, Bayülken A, Bekdemir Ş. Investigation of wind characteristics and wind energy potential in Kirklareli, Turkey. Renew Energ. 2007;32:1739-52.
[73] Dorvlo ASS. Estimating wind speed distribution. Energy Convers Manage. 2002;43:2311-8.
[74] Tuller SE, Brett AC. The goodness of fit of the Weilbull and Rayleigh distribution to the distributions of observed wind speeds in a topographically diverse area. J Climatol. 1985;5:74-94.
[75] Mederos ACM, Padron JFM, Lorenzo AEF. An offshore wind atlas for the Canary Islands. Renew Sust Energ Rev. 2011;15:612-20.
[76] Cellura M, Cirrincione G, Marvuglia A, Miraoui A. Wind speed spatial estimation for energy planning in Sicily: Introduction and statistical analysis. Renew Energ. 2008;33:1237-50.
[77] Bobée B, Ashkar F. The gamma family and derived distributions applied in hydrology. Littleton, Colorado, USA: Water Resources Publications; 1991.
[78] Bobee B, Perreault L, Ashkar F. Two kinds of moment ratio diagrams and their applications in hydrology. Stochastic Hydrol Hydraul. 1993;7:41-65.
[79] Hosking JRM, Wallis JR. Regional frequency analysis: An approach based on L-Moments. New York: Cambridge University Press; 1997.
[80] Rao AR, Hamed KH. Flood frequency analysis. New York: CRC Press; 2000.
[81] Hosking JRM. L-Moments: Analysis and estimation of distributions using linear combinations of order statistics. J R Stat Soc Ser B. 1990;52:105-24.
[82] Meshgi A, Khalili D. Comprehensive evaluation of regional flood frequency analysis by L- and LH-moments. I. A re-visit to regional homogeneity. Stoch Environ Res Risk Assess. 2009;23:119-35.
[83] Peel MC, Wang QJ, Vogel RM, McMahon TA. The utility of L-moment ratio diagrams for selecting a regional probability distribution. Hydrolog Sci J. 2001;46:147-55.
[84] Seckin N, Haktanir T, Yurtal R. Flood frequency analysis of Turkey using L-moments method. Hydrol Process. 2011;25:3499-505.
[85] Vogel RM, Thomas WO, McMahon TA. Flood-flow frequency model selection in southwestern United States. J Water Resour Plan Manag. 1993;119:353-66.
[86] Vogel RM, Wilson I. Probability Distribution of Annual Maximum, Mean, and Minimum Streamflows in the United States. J Hydraul Eng. 1996;1:69-76.
[87] Yue S, Wang C. Possible regional probability distribution type of Canadian annual streamflow by L-moments. Water Resour Manag. 2004;18:425-38.
[88] El Adlouni S, Ouarda TBMJ. Orthogonal projection t-moment estimators for three-parameter distributions. Advances and Applications in Statistics. 2007;7:193-209.
[89] Abolverdi J, Khalili D. Development of Regional Rainfall Annual Maxima for Southwestern Iran by L-Moments. Water Resour Manag. 2010;24:2501-26.
[90] Adamowski K, Alila Y, Pilon PJ. Regional rainfall distribution for Canada. Atmos Res. 1996;42:75-88.
[91] Hussain Z, Pasha GR. Regional Flood Frequency Analysis of the Seven Sites of Punjab, Pakistan, Using L-Moments. Water Resour Manag. 2008;23:1917-33.
[92] Lee SH, Maeng SJ. Frequency analysis of extreme rainfall using L-moment. Irrigation and Drainage. 2003;52:219-30.
[93] Lee SH, Maeng SJ. Estimation of drought rainfall using L-moments. Irrigation and Drainage. 2005;54:279-94.
[94] Noto LV, La Loggia G. Use of L-Moments Approach for Regional Flood Frequency Analysis in Sicily, Italy. Water Resour Manag. 2008;23:2207-29.
[95] Rahman AS, Rahman A, Zaman MA, Haddad K, Ahsan A, Imteaz M. A study on selection of probability distributions for at-site flood frequency analysis in Australia. Nat Hazards. 2013;69:1803-13.

[96] Zakaria ZA, Shabri A, Ahmad UN. Regional Frequency Analysis of Extreme Rainfalls in the West Coast of Peninsular Malaysia using Partial L-Moments. Water Resour Manag. 2012;26:4417-33.
[97] Zaman MA, Rahman A, Haddad K. Regional flood frequency analysis in arid regions: A case study for Australia. Journal of Hydrology. 2012;475:74-83.
[98] Zin WZW, Jemain AA, Ibrahim K. The best fitting distribution of annual maximum rainfall in Peninsular Malaysia based on methods of L-moment and LQ-moment. Theor Appl Climatol. 2009;96:337-44.
[99] Vogel RM, Fennessey NM. L moment diagrams should replace product moment diagrams. Water Resour Res. 1993;29:1745-52.
[100] Akaike H. Information Theory as an extension of the maximum likelihood principle. second international symposium on information theory. Akademiai kiado, Budapest1973.
[101] Schwarz G. Estimating the Dimension of a Model. The Annals of Statistics. 1978;6:461-4.
[102] Cunnane C. Unbiased plotting positions — A review. Journal of Hydrology. 1978;37:205-22.
[103] Ouarda TBMJ, Ashkar F. Effect of Trimming on LP III Flood Quantile Estimates. J Hydraul Eng. 1998;3:33-42.
[104] Anderson TW, Darling DA. A Test of Goodness of Fit. Journal of the American Statistical Association. 1954;49:765-9.
[105] Gerson M. The Techniques and Uses of Probability Plotting. Journal of the Royal Statistical Society Series D (The Statistician). 1975;24:235-57.
[106] Pearson K. Mathematical Contributions to the Theory of Evolution. XIX. Second Supplement to a Memoir on Skew Variation. Philosophical Transactions of the Royal Society of London Series A, Containing Papers of a Mathematical or Physical Character. 1916;216:429-57.
[107] Greenwood JA, Landwehr JM, Matalas NC, Wallis JR. Probability weighted moments: Definition and relation to parameters of several distributions expressable in inverse form. Water Resour Res. 1979;15:1049-54.
[108] Kendall MG, Stuart A. The advanced theory of statistics. fifth ed. London: Charles Griffin; 1987.
[109] Winchester CB. On estimation of the four-parameter kappa distribution [M.Sc.]. Canada: Dalhousie University (Canada); 2000.
[110] FAO. Irrigation in the Middle East region in figures: AQUASTAT Survey - 2008. Water Report. 2008;34.
[111] Ouarda TBMJ, Charron C, Niranjan Kumar K, Marpu PR, Ghedira H, Molini A, et al. Evolution of the rainfall regime in the United Arab Emirates. Journal of Hydrology. 2014;514:258-70.
[112] Naizghi MS, Ouarda TBMJ. Teleconnections and analysis of long-term wind speed variability in the UAE. Int J Climatol. 2016; DOI: 10.1002/joc.4700.
[113] Hosking JRM. Fortran routines for use with the method of L-moments, version 3.04. Yorktown Heights, N.Y.: IBM Research Division; 1996.
[114] Ashkar F, Ouarda TBMJ. On some methods of fitting the generalized Pareto distribution. Journal of Hydrology. 1996;177:117-41.
[115] Bobée B. The Log Pearson Type 3 Distribution and Its Application in Hydrology. Water Resour Res. 1975;11:681-9.
[116] El Adlouni S, Ouarda TBJM, Zhang X, Roy R, Bobee B. Generalized maximum likelihood estimators for the nonstationary generalized extreme value model. Water Resources Research. 2007;43:W03410.
[117] Ouarda TBMJ, El-Adlouni S. Bayesian Nonstationary Frequency Analysis of Hydrological Variables. JAWRA Journal of the American Water Resources Association. 2011;47:496-505.

Table 1. List of probability density functions, domains, number of parameters and estimation methods used.

Name	Probability density function (f(x))	Domain	Parameters	Estimation method
EV1	$\frac{1}{\alpha}\exp\left[-\frac{x-\mu}{\alpha}-\exp\left(-\frac{x-\mu}{\alpha}\right)\right]$	$-\infty < x < +\infty$	1 location, 1 scale	ML, MM
W2	$\frac{k}{\alpha}\left(\frac{x}{\alpha}\right)^{k-1}\exp\left[-\left(\frac{x}{\alpha}\right)^{k}\right]$	$0 \le x \le \infty$	1 scale, 1 shape	ML, MM
G	$\frac{\alpha^k}{\Gamma(k)}x^{k-1}\exp(-\alpha x)$	$0 \le x \le \infty$	1 scale, 1 shape	ML, MM
LN2	$\frac{1}{x\alpha\sqrt{2\pi}}\exp\left[-\frac{(\ln x-\mu)^2}{2\alpha^2}\right]$	$0 \le x \le \infty$	1 location, 1 scale	ML, MM
W3	$\frac{k}{\alpha}\left(\frac{x-\mu}{\alpha}\right)^{k-1}\exp\left[-\left(\frac{x-\mu}{\alpha}\right)^{k}\right]$	$\mu \le x \le \infty$	1 location, 1 scale, 1 shape	ML
LN3	$\frac{1}{(x-m)\alpha\sqrt{2\pi}}\exp\left\{-\frac{\left[\ln(x-m)-\mu\right]^2}{2\alpha^2}\right\}$	$m \le x \le \infty$	2 location, 1 scale	ML, MM
GEV	$\frac{1}{\alpha}\left[1-\frac{k}{\alpha}(x-u)\right]^{\frac{1}{k}-1}\exp\left\{-\left[1-\frac{k}{\alpha}(x-u)\right]^{1/k}\right\}$	$u+\alpha/k \le x < \infty$ if $k<0$ $-\infty < x \le u+\alpha/k$ if $k>0$	1 location, 1 scale, 1 shape	ML, MM
GG	$\frac{\lvert h\rvert\alpha^{hk}}{\Gamma(k)}x^{hk-1}\exp(-\alpha x)^h$	$0 \le x \le \infty$	1 scale, 2 shape	ML, MM
P3	$\frac{\alpha^k}{\Gamma(k)}(x-\mu)^{k-1}\exp\left[-\alpha(x-\mu)\right]$	$\mu \le x \le \infty$	1 location, 1 scale, 1 shape	ML, MM
LP3	$\frac{g\lvert\alpha\rvert}{x\Gamma(k)}\left[\alpha(\log_a x-\mu)\right]^{k-1}\exp\left[-\alpha(\log_a x-\mu)\right]$ where $g=\log_a e$	$e^{\mu/g} \le x < \infty$ if $\alpha>0$ $0 \le x \le e^{\mu/g}$ if $\alpha<0$	1 location, 1 scale, 1 shape	GMM
KAP	$\alpha^{-1}[1-k(x-\mu)/\alpha]^{1/k-1}[F(x)]^{1-h}$ where $F(x)=(1-h(1-k(x-\mu)/\alpha)^{1/k})^{1/h}$	$\infty \le x \le \mu+\alpha/k$ if $k>0$ $\mu+\alpha(1-h^{-k})/k \le x < \infty$ if $h>0$ $\mu+\alpha/k \le x \le \infty$ if $h \le 0, k<0$	1 location, 1 scale, 2 shape	LM, ML

μ: location parameter
m: second location parameter (LN3)
α: scale parameter
k: shape parameter
h: second shape parameter (GG, KAP)
$\Gamma(\,)$: gamma function

Table 2. Description of the meteorological stations. Maximum, mean, median, standard deviation (SD), coefficient of variation (C_V), coefficient of skewness (C_S) and coefficient of kurtosis (C_K).

Station Number	Station Name	Altitude (m)	Latitude	Longitude	Period (year/month)	Maximum (m/s)	Mean (m/s)	Median (m/s)	SD (m/s)	C_V	C_S	C_K
1	Al Aradh	178	23.903° N	55.499° E	2007/06 - 2010/08	12.42	2.47	2.20	1.73	0.70	0.97	4.20
2	Al Mirfa	6	24.122° N	53.443° E	2007/06 - 2009/07	17.17	4.28	3.96	2.26	0.53	0.71	3.58
3	Al Wagan	142	23.579° N	55.419° E	2009/08 - 2010/08	12.36	3.67	3.31	2.22	0.61	0.66	3.08
4	East of Jebel Haffet	341	24.168° N	55.864° E	2009/10 - 2010/08	16.41	4.27	3.87	2.35	0.55	0.99	4.47
5	Madinat Zayed	137	23.561° N	53.709° E	2008/06 - 2010/08	18.04	4.10	3.56	2.44	0.60	0.94	3.83
6	Masdar City	7	24.420° N	54.613° E	2008/07 - 2010/08	12.17	3.09	2.67	2.06	0.67	0.70	2.90
7	Sir Bani Yas Island	7	24.322° N	52.566° E	2007/06 - 2010/08	13.95	3.86	3.76	2.14	0.55	0.43	3.06

Table 3. Ranking of D/Ms for all stations based on the goodness-of-fit criteria.

Station	Criteria	Rank of D/M					
		1st	2nd	3rd	4th	5th	6th
Al Aradh	$\ln L$	GG/ML	GG/MM	W3/ML	KAP/ML	W2/ML	W2/MM
	$R^2_{F,c}$	KAP/LM	P3/MM	GG/MM	LN3/MM	GEV/MM	W2/MM
	$R^2_{p,c}$	GG/MM	W3/ML	W2/MM	KAP/LM	LP3/GMM	GG/ML
	χ^2	GG/MM	W2/MM	W3/ML	KAP/LM	GG/ML	LP3/GMM
	KS	GG/MM	KAP/LM	LN3/ML	EV1/ML	GEV/ML	W3/ML
	AD	KAP/LM	P3/MM	LN3/MM	GEV/MM	GG/ML	GG/MM
Al Mirfa	$\ln L$	W3/ML	KAP/ML	KAP/LM	P3/ML	P3/MM	LN3/ML
	$R^2_{F,c}$	KAP/LM	GG/MM	KAP/ML	W2/MM	W2/ML	LP3/GMM
	$R^2_{p,c}$	KAP/LM	KAP/ML	GG/MM	P3/ML	W2/MM	W2/ML
	χ^2	GG/MM	KAP/ML	P3/MM	W2/MM	KAP/LM	W2/ML
	KS	KAP/LM	KAP/ML	GG/MM	W2/MM	LP3/GMM	W3/ML
	AD	KAP/LM	KAP/ML	P3/ML	P3/MM	GG/MM	W2/MM
Al Wagan	$\ln L$	GG/ML	GG/MM	KAP/ML	W3/ML	KAP/LM	W2/ML
	$R^2_{F,c}$	KAP/LM	LP3/GMM	GG/MM	GG/ML	KAP/ML	W3/ML
	$R^2_{p,c}$	KAP/LM	KAP/ML	LP3/GMM	GG/MM	GG/ML	W3/ML
	χ^2	GG/MM	GG/ML	KAP/ML	KAP/LM	W3/ML	LP3/GMM
	KS	KAP/LM	LP3/GMM	KAP/ML	GG/MM	GG/ML	W3/ML
	AD	KAP/LM	GG/MM	KAP/ML	GG/ML	W3/ML	LP3/GMM
East of Jebel Haffet	$\ln L$	KAP/ML	KAP/LM	LN3/ML	P3/ML	LN3/MM	GEV/ML
	$R^2_{F,c}$	KAP/LM	EV1/ML	LN3/ML	KAP/ML	GEV/ML	GEV/MM
	$R^2_{p,c}$	EV1/ML	GEV/ML	EV1/MM	KAP/LM	LN3/ML	GEV/MM
	χ^2	GEV/MM	GEV/ML	LN3/ML	EV1/ML	LN3/MM	KAP/LM
	KS	KAP/LM	LN3/ML	EV1/ML	KAP/ML	GEV/ML	EV1/MM
	AD	EV1/ML	GEV/ML	KAP/LM	LN3/ML	GEV/MM	KAP/ML
Madinat Zayed	$\ln L$	KAP/ML	P3/ML	KAP/LM	LN3/ML	W3/ML	P3/MM
	$R^2_{F,c}$	KAP/LM	LP3/GMM	P3/ML	G/MM	KAP/ML	LN3/ML
	$R^2_{p,c}$	LN3/ML	GEV/ML	P3/ML	KAP/LM	G/MM	KAP/ML
	χ^2	KAP/ML	KAP/LM	P3/ML	LP3/GMM	GG/MM	P3/MM
	KS	KAP/LM	G/MM	LN3/ML	P3/ML	LP3/GMM	KAP/ML
	AD	LN3/ML	P3/ML	KAP/LM	KAP/ML	GEV/ML	EV1/MM
Masdar City	$\ln L$	KAP/ML	GG/ML	GG/MM	W3/ML	W2/ML	W2/MM
	$R^2_{F,c}$	KAP/LM	LP3/GMM	KAP/ML	GG/MM	GG/ML	W3/ML
	$R^2_{p,c}$	KAP/LM	LP3/GMM	KAP/ML	W2/ML	GG/ML	G/ML
	χ^2	LP3/GMM	KAP/ML	GG/MM	GG/ML	KAP/LM	W3/ML
	KS	LP3/GMM	KAP/LM	KAP/ML	GG/MM	GG/ML	W3/ML
	AD	KAP/ML	GG/ML	GG/MM	W2/ML	W3/ML	W2/MM
Sir Bani Yas Island	$\ln L$	GG/ML	W3/ML	GG/MM	KAP/ML	P3/ML	GEV/ML
	$R^2_{F,c}$	KAP/LM	P3/MM	LN3/MM	GEV/MM	GEV/ML	GG/MM
	$R^2_{p,c}$	GG/MM	KAP/LM	W3/ML	P3/MM	LN3/MM	GEV/MM
	χ^2	GG/MM	W3/ML	GG/ML	KAP/ML	P3/MM	KAP/LM
	KS	KAP/LM	GEV/MM	P3/MM	LN3/MM	GEV/ML	P3/ML

	AD	P3/MM	LN3/MM	GEV/MM	GEV/ML	W3/ML	LN3/ML

Table 4. Distribution parameters for each station.

D/M	Station	μ	α	k	h
W3/ML	Al Aradh	-0.06	2.78	1.44	-
	Al Mirfa	-0.13	4.97	2.04	-
	Al Wagan	-0.11	4.24	1.74	-
	East of Jebel Haffet	-0.07	4.90	1.93	-
	Madinat Zayed	-0.08	4.70	1.78	-
	Masdar City	-0.03	3.45	1.51	-
	Sir Bani Yas Island	-0.47	4.89	2.12	-
GG/MM	Al Aradh	-	0.27	0.67	1.83
	Al Mirfa	-	0.23	1.18	1.79
	Al Wagan	-	0.18	0.60	2.32
	East of Jebel Haffet	-	0.45	2.27	1.21
	Madinat Zayed	-	0.27	1.32	1.48
	Masdar City	-	0.18	0.43	2.56
	Sir Bani Yas Island	-	0.16	0.48	2.99
LP3/GMM	Al Aradh	1.05	-5.46	4.33	-
	Al Mirfa	1.23	-9.48	6.33	-
	Al Wagan	1.10	-5.69	3.60	-
	East of Jebel Haffet	1.46	-13.27	11.94	-
	Madinat Zayed	1.33	-9.21	7.44	-
	Masdar City	1.02	-4.34	2.87	-
	Sir Bani Yas Island	1.03	-5.36	2.83	-
KAP/LM	Al Aradh	1.30	1.81	0.13	0.38
	Al Mirfa	2.99	2.31	0.16	0.24
	Al Wagan	1.88	2.89	0.27	0.52
	East of Jebel Haffet	3.14	1.96	0.03	0.07
	Madinat Zayed	2.51	2.40	0.09	0.34
	Masdar City	0.47	3.82	0.42	0.93
	Sir Bani Yas Island	2.86	2.17	0.21	0.11

Table 5. Power density (W/m^2) for each station from the observed wind speed data or from theoretical distributions.

D/M	Al Aradh	Al Mirfa	Al Wagan	East of Jebel Haffet	Madinat Zayed	Masdar City	Sir Bani Yas Island
$\bar{P}_0$	25.79	93.41	67.77	99.00	95.44	45.89	70.36
EV1/ML	25.70	103.73	73.73	101.94	95.19	47.63	86.96
EV1/MM	26.31	96.43	70.42	100.10	97.16	48.03	74.44
W2/ML	29.28	93.54	71.20	96.82	94.99	49.62	76.41
W2/MM	26.30	92.98	69.12	96.77	94.52	47.69	72.07
G/ML	37.17	108.99	86.03	108.81	110.52	58.86	103.83
G/MM	27.13	95.88	71.10	99.86	97.66	49.08	74.35
LN2/ML	98.91	205.96	140.80	185.71	246.62	102.80	210.54
LN2/MM	28.85	99.80	71.87	103.78	102.73	50.14	76.83
W3/ML	27.26	92.73	69.32	96.39	93.66	48.90	71.09
LN3/ML	29.88	96.00	73.94	99.97	101.81	57.39	71.73
LN3/MM	25.78	93.40	67.74	98.95	95.43	45.86	70.38
GEV/ML	28.28	93.97	69.95	99.74	100.87	53.09	70.54
GEV/MM	25.81	93.42	67.79	98.99	95.45	45.90	70.37
GG/ML	25.63	93.08	67.76	97.50	94.73	46.02	70.30
GG/MM	25.80	93.42	67.78	99.06	95.45	45.88	70.35
P3/ML	30.21	95.26	74.09	97.86	97.29	54.84	72.33
P3/MM	25.78	93.38	67.75	99.05	95.41	45.85	70.34
LP3/GMM	25.83	93.45	67.79	99.04	95.46	45.92	70.40
KAP/ML	27.53	94.19	68.72	98.86	95.09	46.74	73.05
KAP/LM	25.45	92.81	67.34	99.46	96.97	45.45	69.74

FIGURES

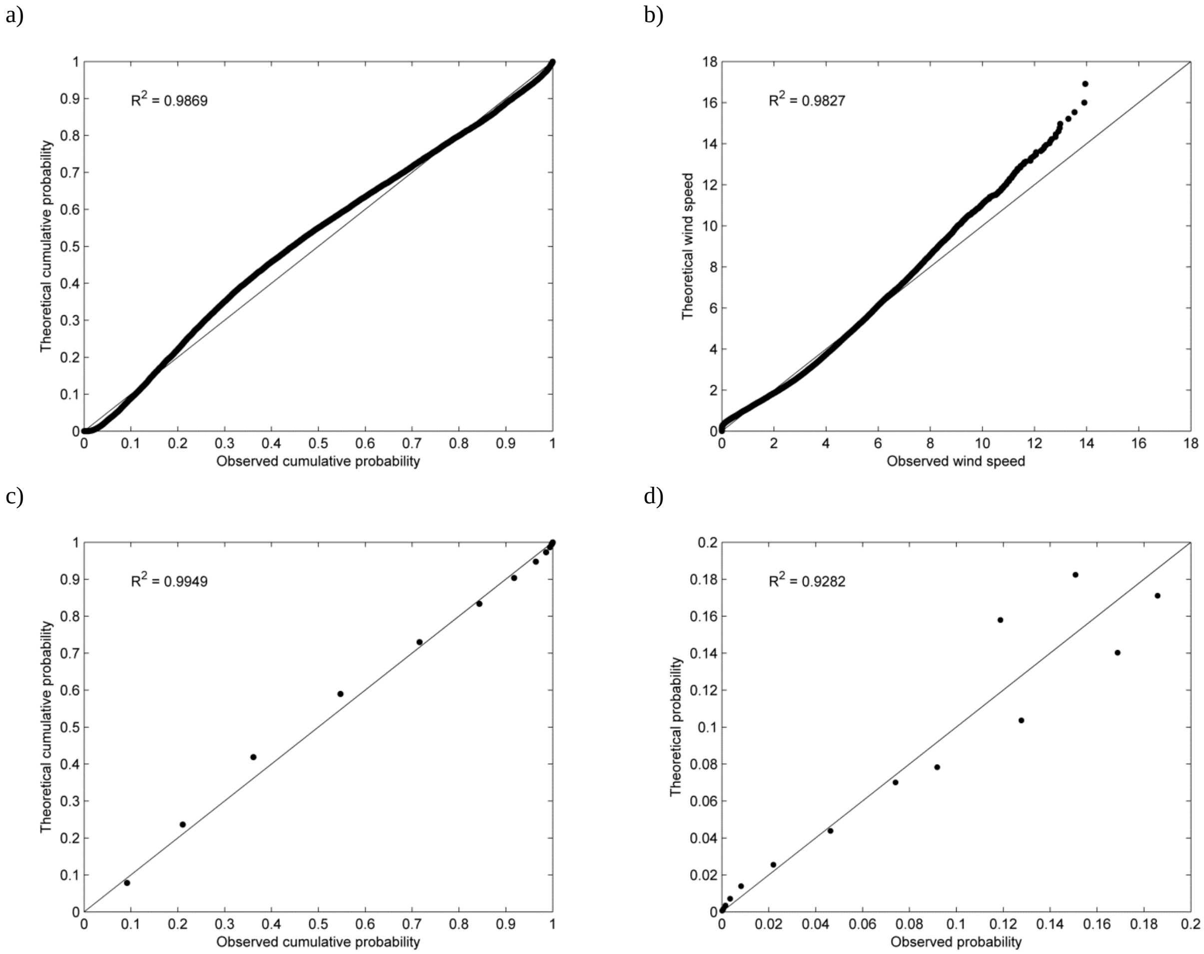

Fig. 1. Examples of a *P*-*P* plot (a), a *Q*-*Q* plot (b), a *P*-*P* plot using the histogram approach (c), and a graph of probabilities at class intervals (d) for the W2 fitted to the wind speed data at Sir Bani Yas. The solid line represents the ideal case where the theoretical distribution is equal to the observed distribution.

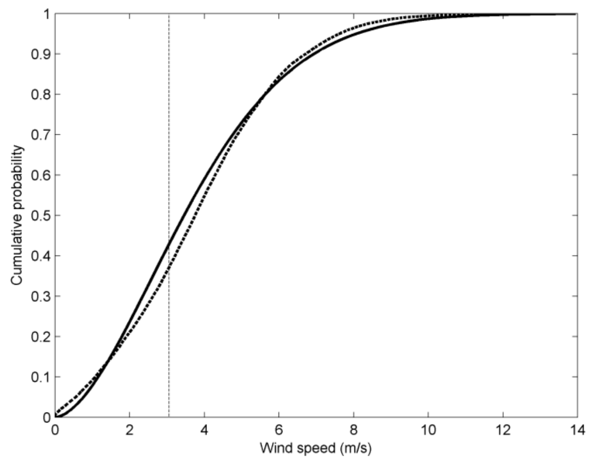

Fig. 2. An example of a theoretical cumulative probability distribution (solid line) and the empirical cumulative probability distribution (dashed line) of the observed wind speed data at Sir Bani Yas. The position of the maximum deviation between both curves is indicated by the vertical thin dashed line.

a) b)

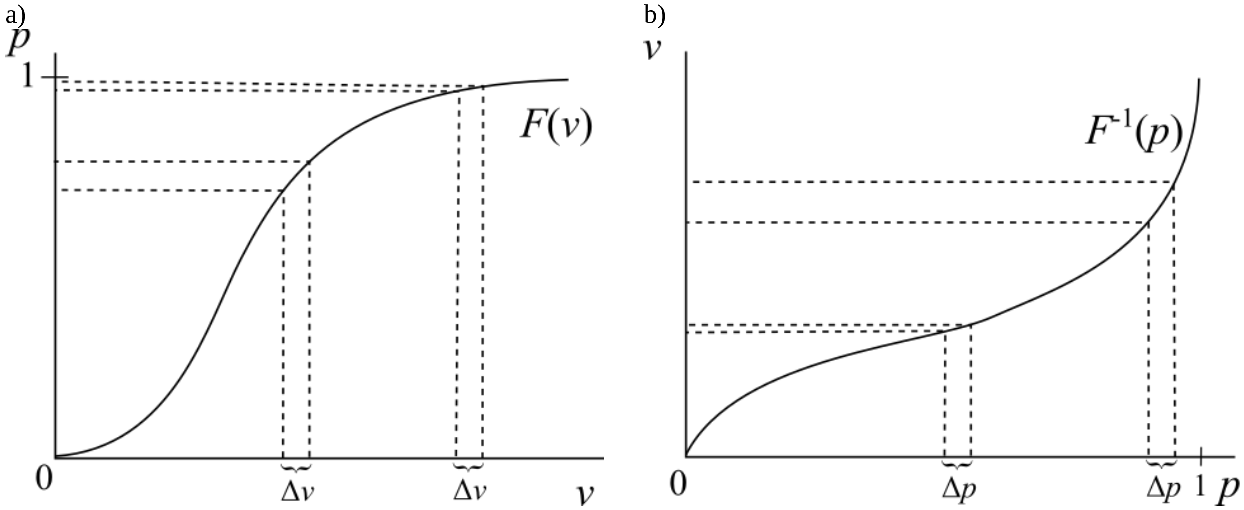

Fig. 3. Hypothetical cumulative distribution function (a) and the inverse hypothetical cumulative distribution function (b).

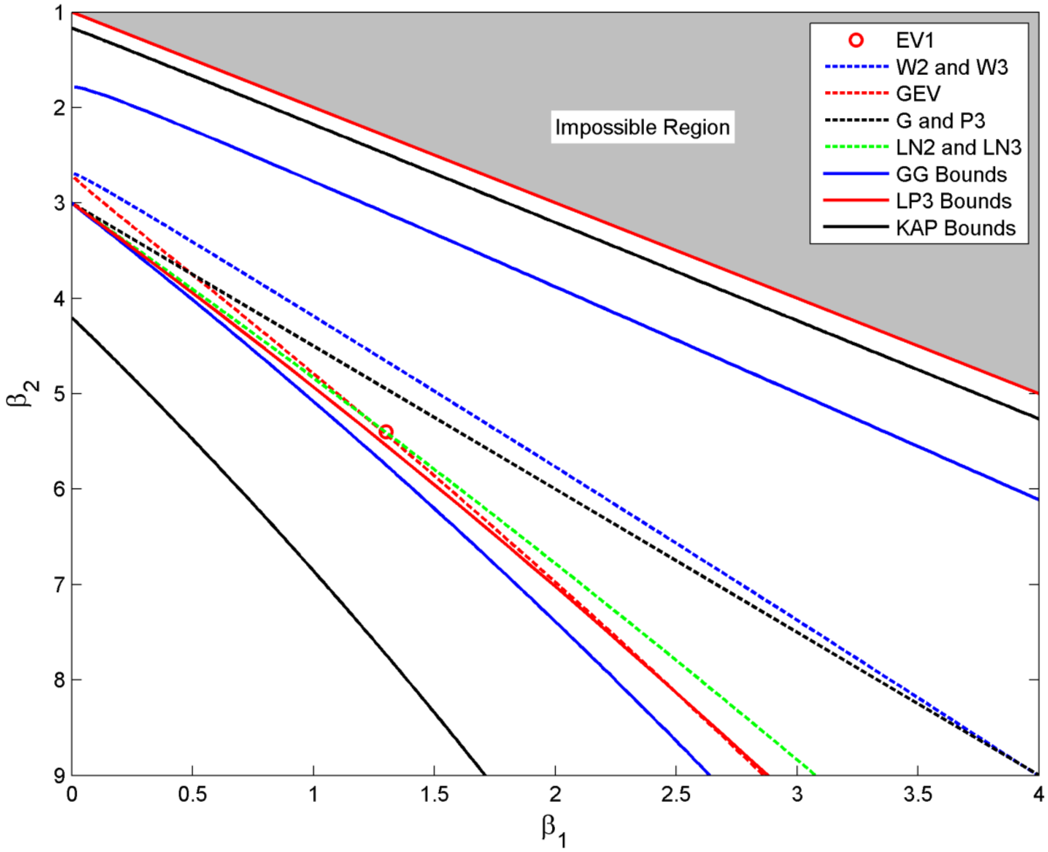

Fig. 4. Moment ratio diagram with selected pdfs. EV1 defines a point, W2, W3, GEV, G, P3, LN2 and LN3 define a curve, and GG, KAP and LP3 define an area.

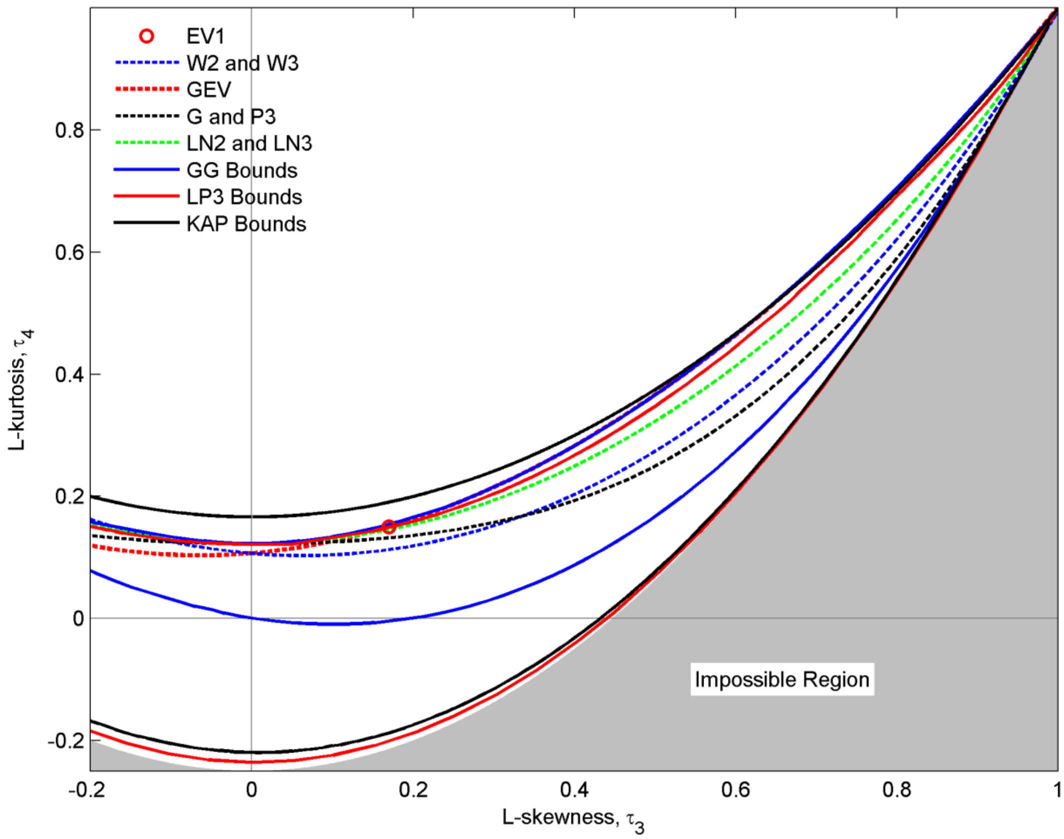

Fig. 5. L-moment ratio diagram with selected pdfs. EV1 defines a point, W2, W3, GEV, G, P3, LN2 and LN3 define a curve, and GG, KAP and LP3 define an area.

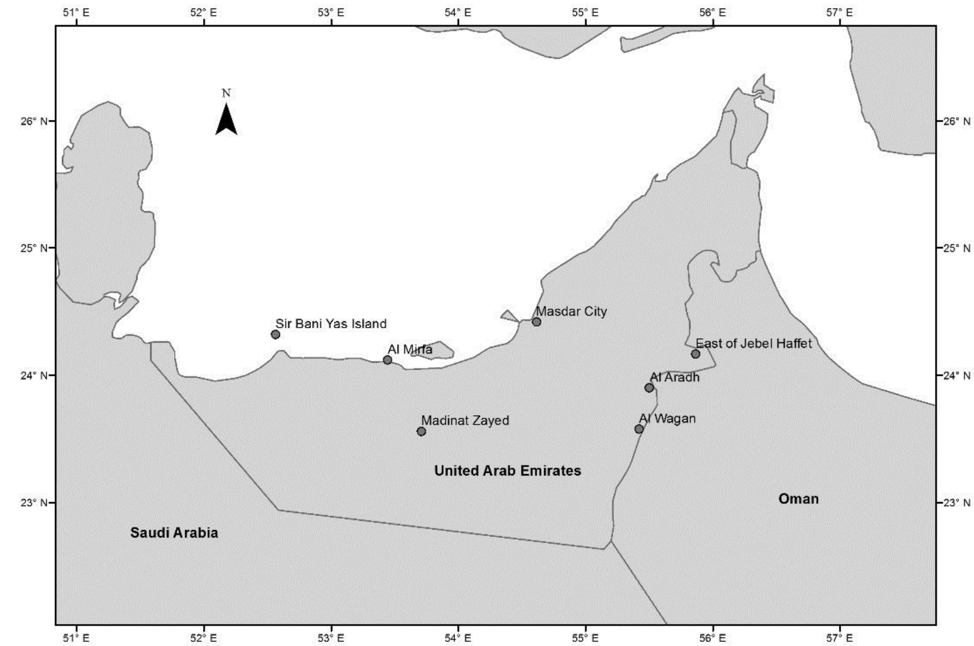

Fig. 6. Geographical location of the meteorological stations.

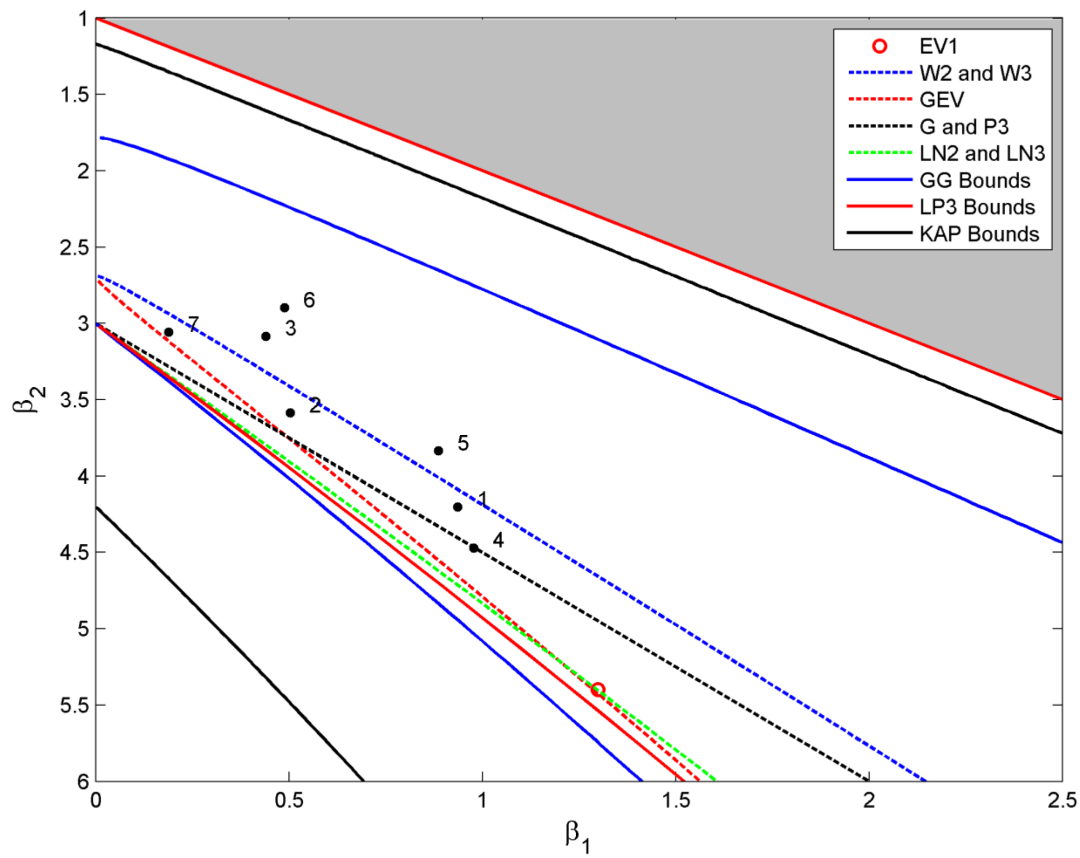

Fig. 7. Moment ratio diagram where each wind station is represented by a dot.

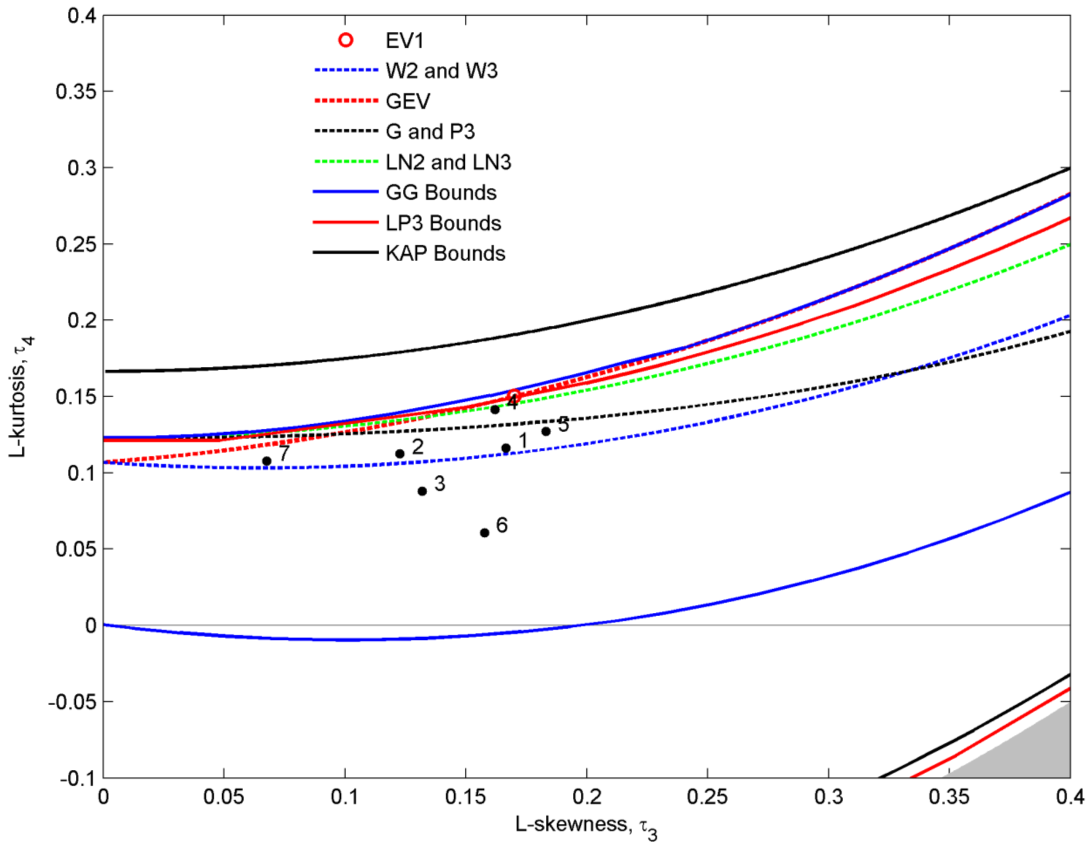

Fig. 8. L-moment ratio diagram where each wind station is represented by a dot.

a)

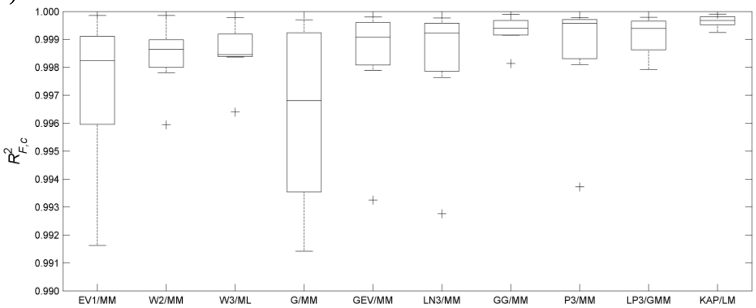

b)

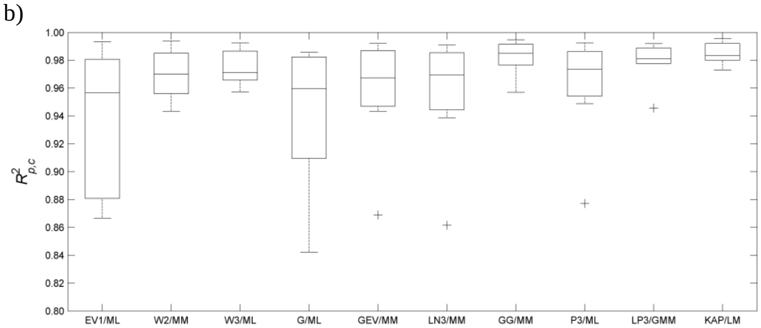

c)

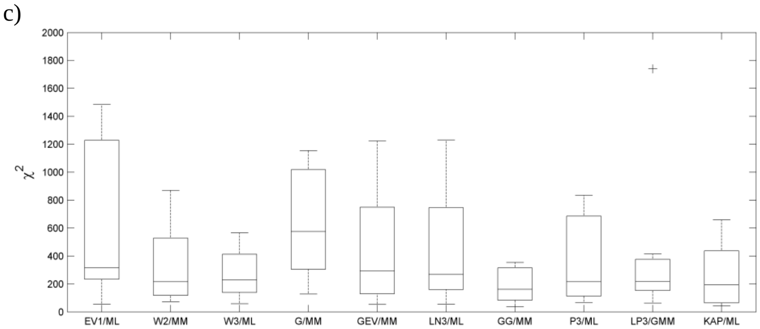

d)

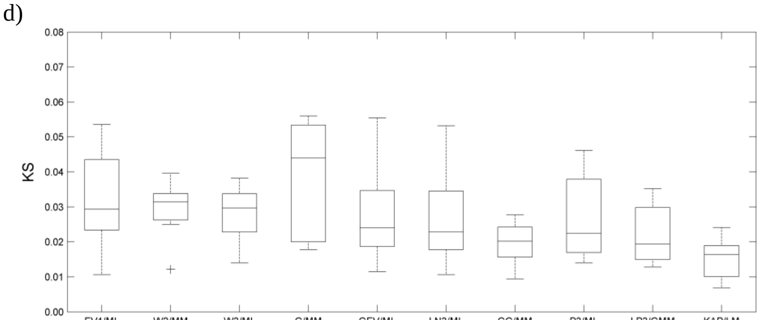

e)

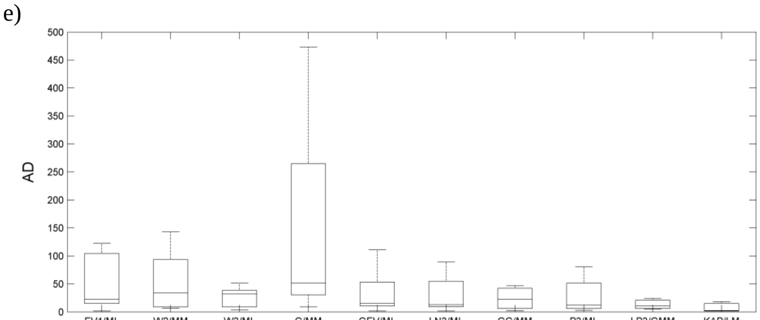

Fig. 9. Box plots of goodness-of-fit criteria: a) $R^2_{F,c}$, b) $R^2_{p,c}$, c) χ^2, d) KS and e) AD.

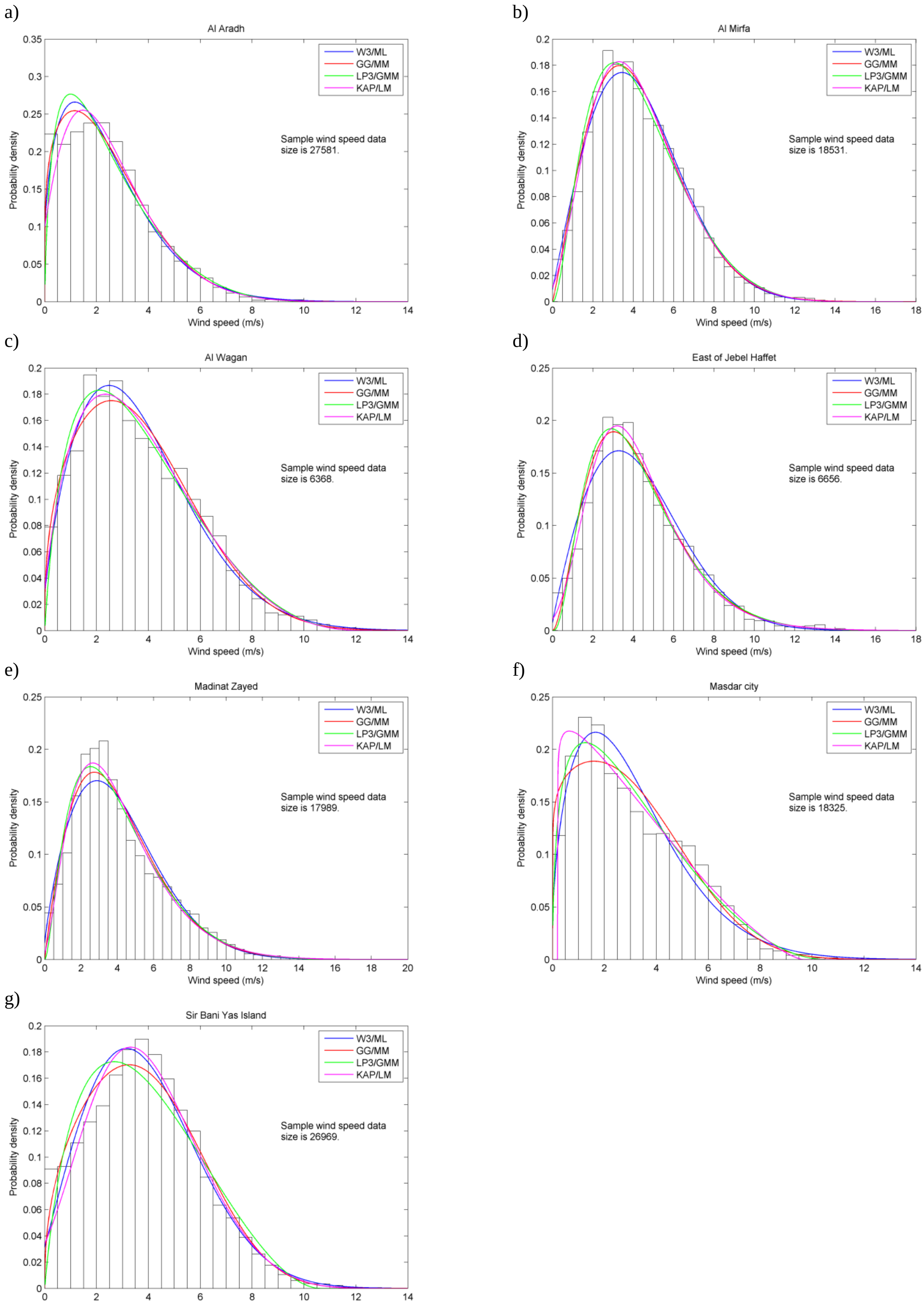

Fig. 10. Wind speed frequency histograms for each station.

a)

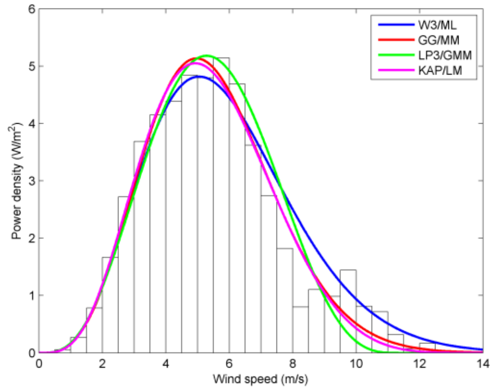
W3/ML
GG/MM
LP3/GMM
KAP/LM
Power density (W/m2)
Wind speed (m/s)

b)

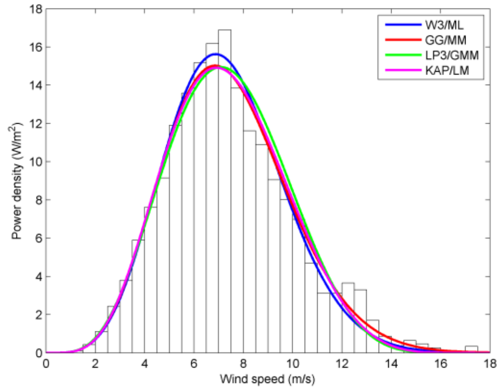
W3/ML
GG/MM
LP3/GMM
KAP/LM
Power density (W/m2)
Wind speed (m/s)

c)

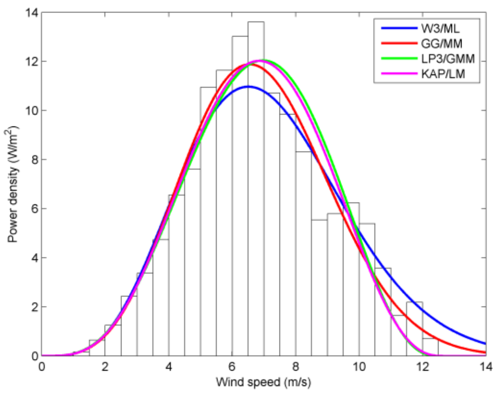
W3/ML
GG/MM
LP3/GMM
KAP/LM
Power density (W/m2)
Wind speed (m/s)

d)

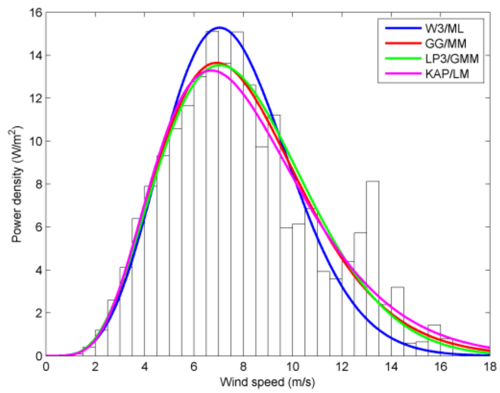
W3/ML
GG/MM
LP3/GMM
KAP/LM
Power density (W/m2)
Wind speed (m/s)

e)

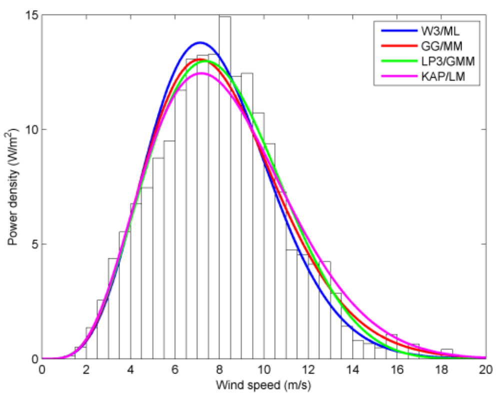
W3/ML
GG/MM
LP3/GMM
KAP/LM
Power density (W/m2)
Wind speed (m/s)

f)

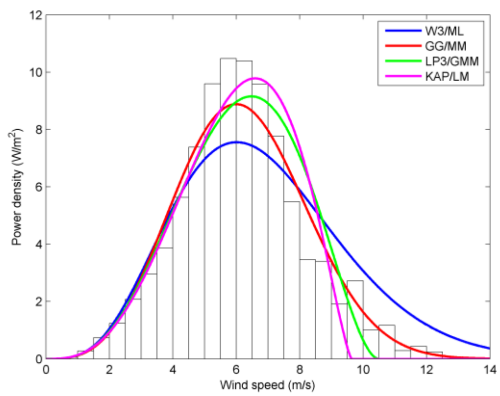
W3/ML
GG/MM
LP3/GMM
KAP/LM
Power density (W/m2)
Wind speed (m/s)

g)

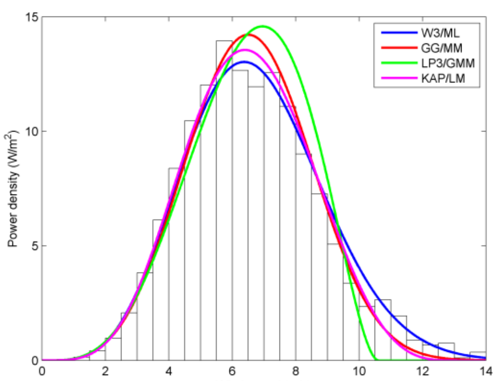
W3/ML
GG/MM
LP3/GMM
KAP/LM
Power density (W/m2)
Wind speed (m/s)

Fig 11. Wind power density histograms for each stations.